Analyses of the Molecular Determinant of Cell Fate Induced by an Antimetabolite, Trifluridine

Yuki KATAOKA

Analyses of the Molecular Determinant of Cell Fate Induced by an Antimetabolite, Trifluridine

A Dissertation Submitted to
the Graduate School of Science and Technology,
University of Tsukuba
in Partial Fulfillment of Requirements
for the Degree of Doctor of Philosophy in Science

Doctoral Program in Biology
Degree Programs in Life and Earth Sciences

Yuki KATAOKA

Table of Contents

Contents		Pages
ABSTRACT		1
ABBREVIATIONS		2
GENERAL INTRODUCTION		4
1.	CHAPTER 1: CYTOTOXICITY OF TRIFLURIDINE CORRELATES WITH THE THYMIDINE KINASE 1 EXPRESSION LEVEL	8
1.1.	Introduction	8
1.2.	Materials and Methods	9
1.2.1.	Cell Culture and Reagents	9
1.2.2.	Plasmid Construction	9
1.2.3.	Generation of *TK1*-knock-out Cell Lines and Cell Lines with Stable and Inducible *TK1* Expression	10
1.2.4.	Western Blot Analysis	10
1.2.5.	Quantitative Reverse-transcription PCR	11
1.2.6.	Cell Viability Assay	11
1.2.7.	Detection of FTD Incorporated in Nuclear DNA	11
1.2.8.	Cell Cycle Analysis	12
1.2.9.	Cytotoxicity Test	12
1.2.10.	Quantitative Real-time Reverse Transcription PCR	12
1.2.11.	Statistical Analysis	13
1.3.	Results	14
1.3.1.	*TK1* Expression is Indispensable for FTD Cytotoxicity	14
1.3.2.	*TK1* knock-out Does Not Affect *AFMID* Expression	15
1.3.3.	*TK1* Expression Level Correlates with FTD Incorporation and Cytotoxicity	15
1.4.	Discussion	18
1.5.	Tables	20
1.6.	Figures	23
2.	CHAPTER 2: DNA REPLICATION STRESS INDUCED BY TRIFLURIDINE DETERMINES TUMOR CELL FATE ACCORDING TO P53 STATUS	32
2.1.	Introduction	32

2.2. Materials and Methods 34
2.2.1. Cell Culture and Reagents 34
2.2.2. DNA Fiber Analysis 34
2.2.3. *In vitro* DNA Polymerase Assay 35
2.2.4. Quantification of dTTP, FTD-TP, and BrdUTP Using LC/triplestage Quadrupole Mass Spectrometry 35
2.2.5. Generation of TP53-deficient HCT 116 Cells 36
2.2.6. Generation of Fluorescent Ubiquitination–based Cell-cycle Indicator-Expressing Cells by Lentiviral Infection 36
2.2.7. Western Blot Analysis 37
2.2.8. Immunofluorescence 37
2.2.9. In Situ Proximal Ligation Assay 37
2.2.10. Image Acquisition 37
2.2.11. Animals and Evaluation of Antitumor Activity *in vivo* 38
2.2.12. Statistical Analysis 38
2.3. Results 39
2.3.1. FTD Stalls Replication Forks and Activates the DNA Damage Response 39
2.3.2. FTD Impedes Replicative DNA Polymerases *In vitro* 39
2.3.3. FTD Rapidly Decreases dTTP and Increases FTD-TP in the Cellular dNTP Pool 40
2.3.4. FTD Induces FancD2 Monoubiquitination During S-phase and Results in the Accumulation of Persistent ssDNA 40
2.3.5. FTD Induces Senescence in Tumor Cells with Wild-type p53 and Apoptosis in p53 Knockout Tumor Cells 41
2.3.6. Cell Fate is Determined According to p53 Status at the G_2-M Transition Following an FTD-induced Extended S-G_2 Phase 43
2.3.7. Severe Chromosomal Bridges are Induced by FTD During Late Mitosis in p53-null Cells 43
2.4. Discussion 45
2.5. Table 48
2.6. Figures 49
GENERAL DISCUSSION 62
ACKNOWLEDGEMENTS 64
REFERENCES 65

Abstract

Trifluridine (FTD) is the antitumoral component of FTD/Tipiracil (TPI), which is classified as an antimetabolite. FTD is phosphorylated by the thymidine salvage pathway, and FTD triphosphate (FTD-TP) is massively incorporated into DNA, which exerts antitumor effect via DNA damage. Since thymidine kinase 1 (TK1) is the first kinase that phosphorylates FTD in cytosol, TK1 is assumed to be an indispensable factor for FTD to exert its antitumor effect. However, the importance of TK1 has not been fully established. Moreover, although FTD was assumed to exert antitumor effect by inducing DNA dysfunction after incorporation into DNA, the cellular phenotype induced by FTD was not analyzed in detail. In this study, I established *TK1*- and *p53*-specific-knock-out human colorectal cancer cell lines and evaluated FTD sensitivity of these cells. The cellular FTD sensitivity was found to depend on the TK1 expression level; in addition, FTD induced cellular senescence or apoptosis, depending on the p53 status, following aberrant mitosis. TK1 is usually highly expressed in tumor cells compared to in normal cells, and loss of p53 activity has been reported to be involved in the acquisition of resistance to various antitumor drugs in many cancer cells. These results indicate that FTD/TPI is an efficient antitumor drug to treat a broad range of tumors.

Abbreviations

ADP:	Adenosine diphosphate
ATM:	Ataxia telangiectasia mutated
ATP:	Adenosine triphosphate
ATR:	Ataxia telangiectasia and Rad3-related
ATRIP:	ATR-interacting protein
BrdU:	Bromodeoxyuridine
BrdUTP:	Bromodeoxyuridine triphosphate
BSA:	Bovine serum albumin
cDNA:	Complementary DNA
CldU:	Chlorodeoxyuridine
dAMP:	Deoxyadenosine monophosphate
DAPI:	4', 6-diamidino-2-phenylindole, dihydrochloride
dATP:	Deoxyadenosine triphosphate
dCTP:	Deoxycytidine triphosphate
dGTP:	Deoxyguanosine triphosphate
DMEM:	Dulbecco's modified Eagle's medium
DNA:	Deoxyribonucleic acid
Dox:	Doxycycline
DRS:	DNA replication stress
DTT:	Dithiothreitol
dTDP:	Deoxythymidine diphosphate
dTMP:	Deoxythymidine monophosphate
dTTP:	Deoxythymidine triphosphate
dUDP:	Deoxyuridine diphosphate
dUMP:	Deoxyuridine monophosphate
dUTP:	Deoxyuridine triphosphate
EDTA:	Ethylenediaminetetraacetic acid
FA:	Fanconi anemia
FBS:	Fetal bovine serum
FTD:	Trifluridine
FTD-DP:	Trifluridine diphosphate
FTD-MP:	Trifluridine monophosphate
FTD-TP:	Trifluridine triphosphate
Fucci:	Fluorescent ubiquitination-based cell-cycle indicator
gRNA:	Guide RNA
KO:	Knock-out
IC_{50}:	50% inhibitory concentration
IdU:	Iodedeoxyuridine
IQR:	Interquartile range
mRNA:	Messenger RNA
OA:	Orotic acid
OMP:	Orotidine monophosphate
PCNA:	Proliferating cell nuclear antigen

PCR:	Polymerase chain reaction
PFA:	Paraformaldehyde
PLA:	Proximity ligation assay
PMSF:	Phenylmethylsulfonyl fluoride
Pol:	DNA polymerase
PRPP:	Phosphoribosyl diphosphate
RAD:	Radiation sensitive
RNA:	Ribonucleic acid
RPA:	Replication protein A
RT-PCR:	Reverse-transcription PCR
RT-qPCR	Quantitative real-time reverse transcription PCR
SA-β-gal:	Senescence-associated β-galactosidase
SD:	Standard diviation
SDS:	Sodium dodecyl sulphate
SDS-PAGE:	SDS-polyacrylamide gel electrophoresis
ssDNA:	Single-stranded DNA
TK1:	Tymidine kinase 1
TOPBP1:	DNA topoisomerase II binding protein 1
TPI:	Tipiracil
UFB:	Ultrafine DNA bridges
UDP:	Uridine diphosphate
UMP:	Uridine monophosphate
UR-DNA:	Under-replicated DNA
UTP:	Uridine triphosphate
5-FU:	5-Fluorouracil

General Introduction

Accurate DNA replication is essential for life functions. However, genomic DNA is constantly exposed to various DNA replication stresses (DRSs). DRSs induce DNA replication arrest, mutations, and DNA strand breaks, which lead to genome instability that is closely related to cancer formation. DRS hampers the maintenance and inheritance of accurate genomic information; therefore, living organisms have developed various types of protective mechanism against DRS. The tumor suppressor p53, often referred to as the guardian of the genome, is a transcription factor that induces the expression of numerous genes that mediate DNA repair or apoptosis, among other biological functions. The induction of senescence, a cellular state during which the cell cycle is arrested and the cells become resistant to cell death, is one of the important roles of p53.

DRS causes a series of phenomena, such as the activation of p53 and its downstream pathways including induction of p21 expression, degradation of mitotic regulators, and induction of mitosis skip, following which senescence is induced [1]. In addition, various mutations of the *p53* gene have been observed in tumor cells, and *p53* mutations contribute towards the resistance to antitumor drugs [2]. Therefore, p53 is considered to influence not only the DNA-damage response but also antitumor treatment (Fig. 1). Antimetabolites, represented by nucleoside analogs such as 5-fluorouracil (5-FU), are a type of anticancer drug that exert antitumor effect by inhibiting cellular division via inducing DRS. For example, 5-FU inhibits thymidylate synthase leading to depletion of thymidine triphosphate a component of DNA [3], and some drugs such as gemcitabine are incorporated into DNA during replication by DNA polymerase; DNA polymerization was observed to be arrested after the incorporation of the abnormal nucleoside [4-6].

Trifluridine, a fluorinated thymidine analog, is the antitumoral component of FTD/TPI that is an antimetabolite used in refractory metastatic colorectal [7] and gastric [8] cancer treatment. FTD is phosphorylated via the thymidine salvage pathway in cytosol and the triphosphate form is massively incorporated into DNA [9, 10]. The incorporated

FTD induces DRS and exerts antitumor effect. TK1 mediated the first phosphorylation step of FTD in thymidine salvage pathway (Fig. 2) [11]. Because of its role, TK1 was assumed to be indispensable for FTD to exert cytotoxicity, but this assumption was not fully proved. To demonstrate the relationship between cellular FTD sensitivity and *TK1* expression level, studies using a *TK1*-specific-deficient human cancer cell line had to be conducted. Furthermore, FTD was found to activate the p53-p21 pathway, leading to sustained cell-cycle arrest with 4N DNA content in the p53-proficient cancer cell line [12]. Because a similar phenotype was observed when cells entered senescence [1], FTD is considered to induce senescence on p53-proficient cancer cells. However, further verification is required to prove that cellular senescence occurs in p53-proficient cells, and the precise events in p53-deficient cancer cells remain unclear.

In this study, I established *TK1*-KO and *TK1* expression-inducible cell lines and demonstrated that *TK1* is an indispensable factor for FTD to exert cytotoxicity, and the cellular FTD sensitivity is correlated with *TK1* expression level. Moreover, FTD was clarified to be incorporated into DNA instead of thymidine. However, the incorporation efficiency was lower than that of thymidine, and even the incorporated FTD interfered with DNA replication as a template DNA strand. Furthermore, I also demonstrated the cellular phenotype induced by FTD using p53-wild cancer cell and newly established its *p53*-KO cell lines. In case the cellular p53 status was wild-type, the p53-p21 pathway was activated by FTD treatment, and senescence following mitosis skip was observed. Moreover, aberrant mitosis was induced in p53-deficient cells, and the cells apoptosed. These data indicate that FTD is an efficient anticancer drug that can be used against various cancers.

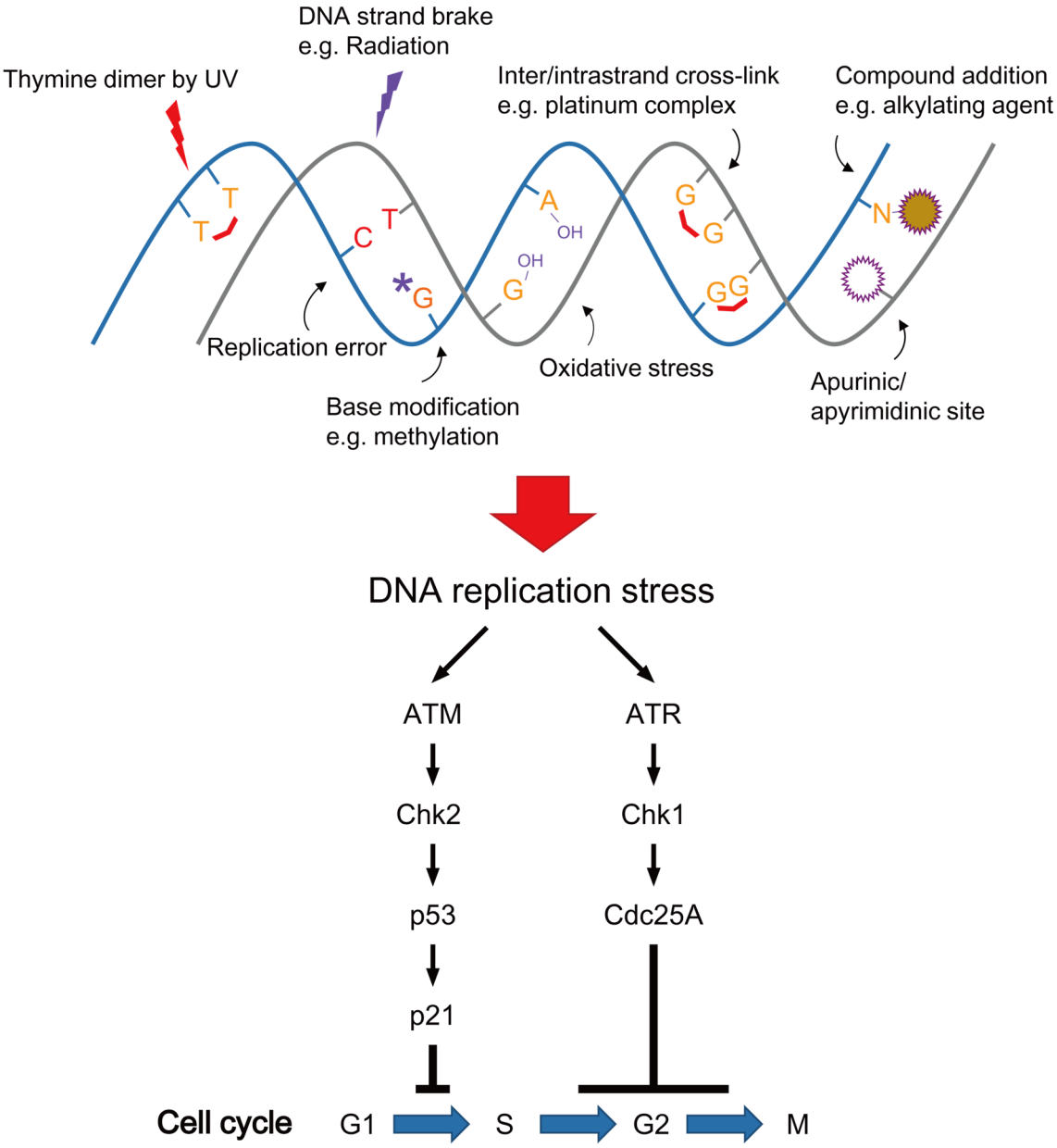

Figure 1: Examples of DNA Damage and Cellular DNA-damage Response.

Various types of DNA damage cause DRS. DRS is recognized by the DNA-damage sensor kinases, ATM and ATR, and the signal is transduced to the effector kinases, Chk1 and Chk2.

Then cell cycle arrest is induced by p53-p21 or Cdc25A activation.

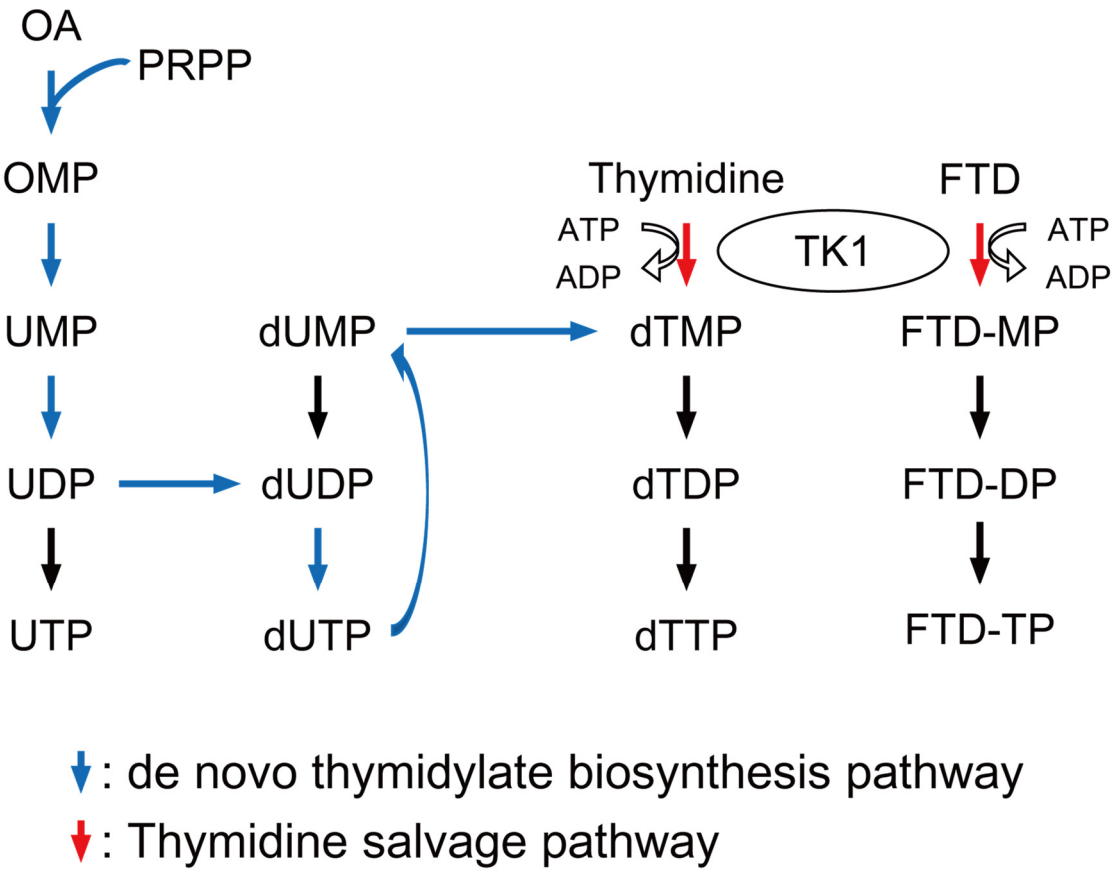

Figure 2: Schematic View of the Pyrimidine Biosynthesis Pathway.

Thymidine is phosphorylated by TK1 in salvage pathway. FTD is also phosphorylated by TK1.

1. Chapter 1: Cytotoxicity of Trifluridine Correlates with the Thymidine Kinase 1 Expression Level

1.1. Introduction

Trifluridine (FTD), a tri-fluorinated thymidine analogue, is a key component of the novel oral antitumor drug FTD/Tipiracil (TPI); based on international phase III clinical trials, this drug can be used to treat refractory metastatic colorectal cancer [7] and metastatic gastric cancer [8]. The tri-phosphorylated form of FTD [9] is reported to be incorporated into DNA through its replication during the S phase [9, 10, 12], resulting in DNA dysfunction and cytotoxicity.

Thymidine kinase 1 (encoded by *TK1* [13]) is a cytosolic nucleoside kinase that is part of the thymidine salvage pathway and mainly phosphorylates thymidine [14, 15]. Based on its chemical structure, FTD is reported to be phosphorylated by TK1, and this modification is suggested to be essential for its cytotoxicity. Indeed, TK1 seems to be associated with the cytotoxicity of FTD [16, 17]; however, the cell lines used in these previous reports were generated by random mutagenesis and not fully validated. Furthermore, although TK1-deficient cells play a key role in determining the importance of TK1 for FTD cytotoxicity, TK1-specific-deficient human cancer cell lines have not been established.

This study generated *TK1*-specific-knock-out human colorectal cancer cell lines and demonstrated that TK1 is essential for cellular sensitivity to FTD. Moreover, to the best of my knowledge, I have provided the first evidence that the *TK1* expression level correlates with FTD sensitivity.

1.2. Materials and Methods

1.2.1. Cell Culture and Reagents

HCT 116 (ECACC; 91091005), HCT 116 (ATCC; CCL-247), HT-29 (ATCC; HTB-38), LoVo (ATCC; CCL-229), LS1034 (ATCC; CRL-2158), LS411N (ATCC; CRL-2159), RKO (ATCC; CRL- 2577), SW48 (ATCC; CCL-231), and SW480 (ATCC; CCL-228) cells were cultured in high-glucose Dulbecco's modified Eagle's medium (DMEM) containing 4 mmol/L L-glutamine and 1 mmol/L sodium pyruvate (Thermo Fisher Scientific) and supplemented with 10% Tet-tested FBS (Thermo Fisher Scientific), 100 U/mL penicillin, and 100 μg/mL streptomycin (Nacalai Tesque) at 37°C in 5% CO_2. FTD was purchased from Tokyo Chemical Industry. Doxycycline was purchased from Takara-Clontech. All reagents were solubilized in distilled water. *TK1*-specific siRNA was synthesized by Thermo Fisher Scientific and the sequence is provided in Table 1-1. In RNAi experiments, Stealth RNAi Negative Control Med GC (Thermo Fisher Scientific) was used as a control and siRNA was transfected using Lipofectamine RNAiMAX (Thermo Fisher Scientific).

1.2.2. Plasmid Construction

To knockout *TK1* using the CRISPR/Cas9 genome editing system, guide RNA (gRNA) sequences were designed using the online software CRISPRdirect [18]. The targeting sequences of gRNAs are provided in Fig. 1-1A and Table 1-1. The sense and antisense oligonucleotides were annealed and cloned into the BbsI site of pX330-U6-Chimeric_BB-CBh-hSpCas9 (Addgene plasmid #42230), which was a gift from Feng Zhang [19]. Donor vectors were constructed using PCR; template DNA (genomic DNA of HCT 116 cells) was amplified using KOD FX DNA polymerase (TOYOBO) and primers containing a sequence homologous to the target locus, which are provided in Table 1-1. The amplified left- and right-arm DNA fragments, which contained approximately 600–700 base pairs homologous to the target locus, and a puromycin resistance cassette were cloned into the BamHI–NotI site of pBluescript SK+ using an In-Fusion HD Cloning Kit (Takara-Clontech). To construct the stable and inducible *TK1* expression plasmids, the *TK1* gene was amplified from template DNA (total cDNA of HCT 116 cells) using KOD FX DNA polymerase (TOYOBO) and

primers (Table 1-1), and then cloned into the pcDNA3.1 (Thermo Fisher Scientific) and pTetOne (Takara-Clontech) vectors using an In-Fusion HD Cloning Kit (Takara-Clontech), respectively.

1.2.3. Generation of *TK1*-knock-out Cell Lines and Cell Lines with Stable and Inducible *TK1* Expression

To establish *TK1*-KO cells, HCT 116 and RKO cells were co-transfected with a CRISPR-Cas9 vector and donor vector. Forty-eight hours later, cells were selected with 500 ng/mL puromycin (Thermo Fisher Scientific). The puromycin resistance cassettes integrated into the *TK1* loci were removed using the Cre-*loxP* recombination system (Fig. 2B). Cre recombinase proteins were delivered into *TK1*-KO cells using Cre Recombinase Gesicles (Takara-Clontech). To establish cells with stable *TK1* expression, RKO cells were transfected with the pcDNA3.1-TK1 plasmid. Forty-eight hours later, cells were selected with 500 μg/mL G418 (Geneticin; Thermo Fisher Scientific). To establish cells with inducible *TK1* expression, *TK1*-KO HCT 116 and RKO cells were co-transfected with a 50:1 ratio of pTetOne-TK1: linear hygromycin marker, according to the manufacturer's protocol (Takara-Clontech). Forty-eight hours later, cells were selected with 400 μg/mL hygromycin B (Thermo Fisher Scientific). All transfections were carried out using the 4D Nucleofector system (Lonza).

1.2.4. Western Blot Analysis

Cells were lysed in RIPA buffer [50 mM Tris-HCl (pH 8.0), 150 mM NaCl, 1.0% Nonidet P-40, 0.5% sodium deoxycholate, and 0.1% SDS] containing 1 mM phenylmethylsulfonyl fluoride and appropriate concentrations of a protease inhibitor cocktail (Nacalai Tesque) and a phosphatase inhibitor cocktail (Nacalai Tesque). Cell extracts were clarified by centrifugation. The supernatant was boiled in SDS sample buffer (Nacalai Tesque). An ImageQuant LAS-4000 mini system (GE Healthcare) was used to detect chemiluminescence. Signal intensities were quantified using ImageQuant TL software (GE Healthcare). The following antibodies were used at the indicated dilutions: anti-TK1 (1:5000; clone EPR3193, Abcam) and anti-β-actin (1:10,000; clone AC-74, Sigma). Images were cropped for presentation.

1.2.5. Quantitative Reverse-transcription PCR

Total RNA was extracted from each cell line using an RNeasy Mini Kit (Qiagen). cDNA was synthesized with a High-Capacity cDNA Reverse Transcription Kit (Applied Biosystems) using the primers provided in Table 1-1. mRNA expression was normalized against that of *β-actin*. Quantitative RT-PCR was performed with a QuantiFast SYBRGreen PCR Kit (Qiagen). Fluorescence signals were detected by a LightCycler 480 system (Roche Diagnostics).

1.2.6. Cell Viability Assay

Cell viability was evaluated using the CellTiter-Glo 2.0 Assay (Promega) according to the manufacturer's protocol. Briefly, cells were plated in a 96-well plate at a density of 500 cells per well in 100 μL of growth medium. The next day, 50 μL of growth medium containing 3× final concentration of doxycycline was added to each well. One day later, 50 μL of medium containing 4× final concentration of FTD and the final concentration of doxycycline was added. Three days later, 100 μL of culture medium was removed, 100 μL of CellTiter-Glo 2.0 assay reagent was added, and the sample was agitated to uniformly lyse cells. Luminescence was detected using a TriStar LB941 reader (Berthold Technologies). The ratio of the luminescence of each sample to that of the mock-treated sample was determined, and the half maximal inhibitory concentration (IC_{50}) value was calculated with XLfit (IDBS). The "dose response 205" program was used for curve fitting. Each experiment was repeated thrice. To determine the cell growth rate, the RealTime-Glo MT Cell Viability assay (Promega) was performed according to the manufacturer's protocol. Briefly, cells were treated with an appropriate concentration of MT Cell Viability Substrate and NanoLuc Enzyme. Luminescence was detected by a TriStar LB941 reader at 1 h and various other time points after cell plating.

1.2.7. Detection of FTD Incorporated in Nuclear DNA

FTD was detected as was described previously [20]. Briefly, cell seeding and addition of doxycycline and FTD were performed as described for the cell viability assay. One hour after FTD addition, cells were fixed in ice-cold 70% ethanol for 5 min and treated with 1.5 N HCl for 1 h. After blocking with goat serum, FTD was detected using an

anti-BrdU antibody (1:250; clone 3D4; BD Biosciences). Samples were treated with an Alexa Fluor 488-conjugated goat anti-mouse IgG secondary antibody (1:200; Thermo Fisher Scientific) and 1 μg/mL DAPI (DOJINDO). Fluorescence was detected using a Cytell Cell Imaging System (GE Healthcare). Images were analyzed using IN Cell Analyzer Workstation 3.7.1. The maximum fluorescence intensity in cells cultured without FTD was determined as the background. Outliers and signals less than the background were excluded. To calculate outliers, the upper quartile (Q3/4) and lower quartile (Q1/4) were first determined. Then, the interquartile range (IQR) was calculated as Q3/4 − Q1/4. Data that were more than Q3/4 + 1.5 × IQR or less than Q1/4 − 1.5 × IQR were defined as outliers.

1.2.8. Cell Cycle Analysis

Cells were harvested by trypsinization after 1 day of doxycycline treatment, fixed with 70% ethanol, and stained with propidium iodide. Fluorescence was analyzed using a FACSCalibur instrument (BD Biosciences). The cell cycle was evaluated by DNA content analysis.

1.2.9. Cytotoxicity Test

siRNA-transfected cells were seeded at densities of 1×10^3 (HCT 116 cells) or 3×10^3 (LoVo and SW480 cells) cells/well in 96-well plates, incubated for 24 h, and then treated with FTD for 72 h. Cell numbers were determined using a simplified crystal violet staining method.

1.2.10. Quantitative Real-time Reverse Transcription PCR

Cells were replated 48 h after siRNA transfection. FTD was added at 24 h after replating. mRNA expression was quantified at 0 and 72 h after FTD addition. RT-qPCR was performed on a PRISM 7900HT sequence detection system using TaqMan Universal PCR Master Mix (Applied Biosystems) with the following amplification conditions: 50°C for 2 min, 95°C for 10 min, 40 cycles of 95°C for 15 s, and 60°C for 1 min. The expression level of *TK1* was normalized to those of β-actin (*ACTB*). The primers and TaqMan probes were prepared using Assay-on-Demand gene-expression products (Applied Biosystems). Probe ID was Hs01062123_m1 for *TK1*. The human

ACTB probe (VIC/MGB Probe; Applied Biosystems) was used as an endogenous control.

1.2.11. Statistical Analysis

The statistical analysis was performed using GraphPad Prism (GraphPad Software) software. The two-tailed *t*-test was used in Figs. 1-7A, and B.

1.3. Results

1.3.1. *TK1* Expression is Indispensable for FTD Cytotoxicity

I first examined the relationship between TK1 expression and FTD sensitivity in a panel of colorectal cancer cell lines. The TK1 expression level varied among the cell lines; however, no correlation was observed between TK1 expression and FTD sensitivity (Fig. 1-1A, B). To exclude the possibility that differences in the genetic background among these cell lines influenced the results, I knocked down *TK1* to validate its importance for FTD cytotoxicity. Although *TK1*-knock-down cells had reduced sensitivity to FTD, it was not markedly different from that of control cells (Fig. 1-1C-F).

To overcome this, I generated *TK1*-specific-KO HCT 116 human colorectal cancer cells using the CRISPR/Cas9 genome editing system using a knock-in strategy. Specifically, the *TK1* gene was targeted at two sites in exons 1 and 4 (Fig. 1-2A), and puromycin resistance gene cassettes were integrated into the genome via homologous recombination (Fig. 1-2B). I obtained two puromycin-resistant HCT 116 cell lines; exons 1 and 4 were targeted in HCT 116/TK1KO ex.1 cells and HCT 116/TK1KO ex.4 cells, respectively. TK1 protein expression was completely abolished in both cell lines (Fig. 1-2C).

To evaluate FTD sensitivity, HCT 116 parental and TK1-KO cells were treated for 3 days with a dilution series of FTD comprising nine concentrations and then their viability was determined. The HCT 116/TK1KO cell lines were more than 100-fold less sensitive to FTD than HCT 116 parental cells (Fig. 1-2D, Table 1-2). The growth curve, doubling time (Fig. 1-2E), and cell cycle distribution (Fig. 1-2F) of HCT 116/TK1KO cells were similar to those of HCT 116 parental cells; therefore, the difference in FTD sensitivity between these two cell lines was due to their disparate *TK1* expression levels. *TK1*-KO RKO cells were also resistant to FTD (Fig. 1-3). Furthermore, a similar result was recently reported in *TK1*-KO DLD-1 cells [20], suggesting that TK1 is essential for FTD cytotoxicity in a range of cell lines.

1.3.2. *TK1* knock-out Does Not Affect *AFMID* Expression

TK1 and *AFMID*, which encodes arylformamidase (Afmid, also known as kynurenine formamidase), are located on the same locus (*17q25.3*) and transcribed in opposite directions (Fig. 1-4A). Hence, the KO of *TK1* may affect *AFMID* expression. Indeed, although *TK1*-KO mice have been reported and exhibit kidney failure [21] , they do not express any native *Afmid* mRNA, and Afmid-specific activity is reduced to 0.1% in the liver [22]. The concurrent KO of two genes was unhelpful in determining which gene was responsible for the phenotype. Therefore, I had to ensure that *TK1* was knocked out without affecting *AFMID* expression.

I first analyzed *AFMID* expression in the *TK1*-KO cell lines. The expression of *AFMID* was approximately 30% lower in HCT 116/TK1KO ex.1 and HCT 116/TK1KO ex.4 cells than in HCT 116 parental cells (Fig. 1-4B). I hypothesized that *AFMID* expression may vary between individual cells of the HCT 116 parental line; therefore, I selected clones with lower *AFMID* expression when generating the *TK1*-KO cell lines. To test this hypothesis, I isolated individual HCT 116 cells from the parental line by limiting dilution and analyzed *AFMID* expression in each clone. The *AFMID* expression level varied between these clones (Fig. 1-4C), indicating that the expression level of *AFMID* in HCT 116 parental cells is an average of that in each individual cell.

Alternatively, inserting the puromycin resistance cassettes may have affected *AFMID* expression. To exclude this possibility, I investigated whether the *AFMID* expression level changed after removing the puromycin resistance cassettes from the *TK1* loci using Cre-*loxP* recombination. The removal of these cassettes did not affect *AFMID* expression (Fig. 1-4D). Therefore, the reduced *AFMID* expression in the *TK1*-KO cell lines was due to clonal variation and not due to the insertion of the puromycin resistance cassettes into the *TK1* loci. Thus, I concluded that *TK1*-specific-KO cell lines can be generated without affecting *AFMID* expression.

1.3.3. *TK1* Expression Level Correlates with FTD Incorporation and Cytotoxicity

The relationship between *TK1* KO and cytotoxicity of FTD was described above (Fig. 1-2); however, whether FTD cytotoxicity correlates with the expression level of *TK1* was unknown. To address this question, I first examined FTD cytotoxicity in

TK1-overexpressing RKO cells, in which the basal expression of TK1 was low (Fig. 1-5A). *TK1*-overexpressing RKO cells did not exhibit increased sensitivity to FTD, suggesting that an excess amount of TK1 protein does not enhance FTD sensitivity (Fig. 1-5A, B). I next investigated whether the *TK1* expression level correlates with FTD cytotoxicity when *TK1* expression was lower than the endogenous level. To this end, I generated cells with inducible *TK1* expression (hereafter referred to as HCT 116/TK1tet and RKO/TK1tet cells), in which *TK1* expression was induced by doxycycline treatment using *TK1*-KO cells. In these cells, TK1 expression was efficiently induced by treatment with doxycycline for 1 day, and the expression level correlated well with the concentration of doxycycline (Fig. 1-6A-C). The expression level of TK1 plateaued at 1,000 ng/mL doxycycline and was about one-half of that in HCT 116 parental cells. Without doxycycline treatment, HCT 116/ TK1tet cell lines were resistant to FTD, similar to *TK1*-KO cells (Fig. 1-6D, E). Furthermore, the effect of doxycycline on TK1 expression persisted for 4 days (Fig. 1-6F, G), indicating that TK1 expression was sustained throughout all experiments. The HCT 116/TK1tet cell lines grew slightly slower than HCT 116/TK1KO ex.4 and HCT 116 parental cells (Fig. 1-2E). This might be caused by the stable integration of the *TK1* expression-inducible plasmids. Doxycycline did not affect the growth (Fig. 1-2E) or cell cycle distribution (Fig. 1-2F) of any cell line *per se*.

To evaluate whether FTD was incorporated into the genomic DNA of HCT 116/TK1KO ex.4 or HCT 116/ TK1tet cell lines, I treated these cells with 6.4 μmol/L FTD, which was the IC_{50} value when HCT 116 parental cells were treated with FTD for 3 days without doxycycline (Fig. 1-2D and Table 1-2), for 1 h and analyzed the amount of incorporated FTD. Consistent with a previous report [23], FTD was rapidly incorporated into nuclear DNA in HCT 116 parental cells, whereas it was hardly detectable in *TK1*-KO cells, and these results were not affected by adding doxycycline (Fig. 1-6H). In HCT 116/TK1tet cell lines, the amount of incorporated FTD correlated with the doxycycline concentration (Fig. 1-6H, I and Table 1-3). These data indicate that the amount of FTD incorporated into nuclear DNA depends on the *TK1* expression level. As was described above, *TK1*-expressing cells were sensitive to FTD, whereas *TK1*-KO cells were highly resistant to FTD (Fig. 1-2D, 6D, E). Next, I investigated whether FTD cytotoxicity was dependent on the *TK1* expression level. To compare FTD

sensitivity between cell lines, I calculated the IC_{50} values in the presence of various concentrations of doxycycline. While doxycycline did not affect FTD cytotoxicity in HCT 116 parental or *TK1*-KO cells, FTD sensitivity correlated well with the doxycycline concentration in HCT 116/TK1tet cell lines (Fig. 1-6J, K and Table 1-2). FTD sensitivity also correlated with the doxycycline concentration in RKO/TK1tet cell lines (Fig. 1-7A, B). These results indicated that the *TK1* expression level highly correlates with cellular sensitivity to FTD in an isogenic background.

1.4. Discussion

Previously, TK1 was found to be indispensable for FTD cytotoxicity [16, 17]; however, the cells used were not certified as *TK1*-deficient. In this study, I generated *TK1*-specific-KO human cancer cell lines using the CRISPR/Cas9 genome editing system and then obtained cell lines with inducible *TK1* expression; to the best of my knowledge, this is the first time these cells have been generated in this manner. Using these cells, I confirmed that *TK1* was essential for cellular sensitivity to FTD. Furthermore, I demonstrated that the *TK1* expression level correlated with FTD sensitivity.

Although *TK1*-KO mice have been reported, they were also deficient in AFMID, a formamidase that is part of the tryptophan catabolism pathway [21, 22]. *TK1* and *AFMID* are located on the same locus; therefore, KO of *TK1* may affect *AFMID* expression. The simultaneous KO of two genes hinders the elucidation of the function of each gene. Considering the potential influence on *AFMID* expression, I targeted exon 4 of *TK1* to generate *TK1*-KO cells. These cells did not exhibit changes in growth, cell cycle distribution, or *AFMID* expression. Thus, I conclude that the phenotypes of *TK1*-KO cells were due to their lack of *TK1* expression. In comparison with HCT 116 parental cells, *TK1*-KO cells were highly resistant to FTD. This demonstrated that *TK1* expression was indispensable for FTD to exert cytotoxicity and excluded the possibility that AFMID was involved in FTD cytotoxicity.

I found no correlation between TK1 expression and FTD sensitivity in the panel of colorectal cancer cell lines. Furthermore, overexpression of TK1 did not increase the sensitivity of cells to FTD. Other factors, in addition to the TK1 expression level, may determine FTD sensitivity. Indeed, nucleoside transporters (hENT1, hENT2, and hCNT1) [11, 23-25] contribute to FTD cytotoxicity. Furthermore, nucleoside kinases, such as TMPK and NDK, are predicted to be involved in FTD phosphorylation. Hence, the overexpression of TK1 alone is insufficient to increase the sensitivity of cells to FTD. Furthermore, doxycycline-inducible expression of *TK1* increased FTD sensitivity in a doxycycline dose-dependent manner in cells with the same genetic background as *TK1*-KO cells. These results strongly indicate that the *TK1* expression level highly correlates with cellular cytotoxicity to FTD in an isogenic background, because the *TK1*

expression level was dependent on the doxycycline concentration, and doxycycline did not affect cell growth or the cell cycle. Together, these data suggest that FTD would more effectively treat cancers with high *TK1* expression than those with low *TK1* expression.

Thymidine kinase activity was higher in the tumor than in normal tissue from the same patient [26]. Furthermore, high expression of *TK1* significantly correlates with poor prognosis in various types of cancer, and the *TK1* expression level is thus considered to be a prognostic factor [27-31]. Cancers that highly express *TK1* may be efficiently treated using FTD/TPI. Recently, the importance of the TK1 expression level as a predictive factor of FTD/TPI efficacy in metastatic colorectal cancer patients has been discussed [32, 33]. Future studies should determine the expression levels of *TK1* in clinical specimens of various types of cancer. These findings are expected to help determine which types of cancer are particularly susceptible to FTD/TPI treatment.

1.5. Tables

Table 1-1: Primer, gRNA and siRNA Sequences.

gRNA for pX330

Primer	Sequence (5′ - 3′)
TK1_KO_exon1_sense	CACCGAATGCAGCTCATTGCGCCTC
TK1_KO_exon1_antisense	AAACGAGGCGCAATGAGCTGCATTC
TK1_KO_exon4_sense	CACCGGCTGTCATAGGCATCGACGA
TK1_KO_exon4_antisense	AAACTCGTCGATGCCTATGACAGCC

PCR to construct donor vectors

Primer	Sequence (5′ - 3′)
TK1_exon1_L-arm_F	GCAGCCCGGGGGATCCCTGGCAGGGTCTACGGATATTATTAGC
TK1_exon1_L-arm_R	TATACGAACGGTAGGAAGTTCACGAACCCGAGTACTCTCCAA
TK1_exon1_R-arm_F	TATACGAACGGTAGGAGCTGCATTAACCTGCCCACTGT
TK1_exon1_R-arm_R	CGCGGTGGCGGCCGCCCACGGCTTCAGACTCCTTGGTTT
TK1_exon4_L-arm_F	GCAGCCCGGGGGATCCCAGCTCCTGAACAGTGGAAGAGTT
TK1_exon4_L-arm_R	TATACGAACGGTAGGATGCCTATGACAGCCACGCCCAGG
TK1_exon4_R-arm_F	TATACGAACGGTAGGAGTTTGTAAGTTGGCTTGTCTTGGCA
TK1_exon4_R-arm_R	CGCGGTGGCGGCCGCTGTGCGCTGCTATGACTGGCTAATTTCT

PCR of TK1 for insertion into pTetOne

Primer	Sequence (5′ - 3′)
TK1_F	CCCTCGTAAAGAATTCACCATGAGCTGCATTAACCTGCCC
TK1_R	GCAGAGATCTGGATCCTCAGTTGGCAGGGCTGCATTG

Quantitative RT-PCR

Primer	Sequence (5′ - 3′)
TK1_F	GGCAGTTTTTCCCTGACATC
TK1_R	CCTCGACCTCCTTCTCTGTG
AFMID_F	ACTGGGAGCAGAGGAAGCCTTGA
AFMID_R	GACATGCAGCAGGCTCTTCCT
β-actin_F	CTGGCACCACACCTTCTACAATG
β-actin_R	GGCGTACAGGGATAGCACAGC

RNAi

Primer	Sequence (5′ - 3′)
TK1_siRNA	CUCGCUACAGCAGCAGCUUdTdT

Table 1-2: IC_{50} Value of FTD in Each Cell Line.

FTD IC_{50} (Average ± SD, μM)

	Doxycycline (ng/ml)						
Cell line	0	10	20	30	60	100	300
HCT 116	6.4 ± 1.6	-	-	-	-	-	6.0 ± 1.3
HCT 116/TK1KO ex.4	710 ± 47	-	-	-	-	-	670 ± 81
HCT 116/TK1tet cl.1	710 ± 50	470 ± 30	390 ± 36	240 ± 100	99 ± 14	41 ± 4.6	18 ± 4.7
HCT 116/TK1tet cl.2	680 ± 150	530 ± 64	350 ± 42	230 ± 53	170 ± 40	71 ± 10	60 ± 18

Table 1-3: Incorporation of FTD into DNA.

Cell line	HCT 116			HCT 116/TK1KO ex.4		
FTD (μM)	0	6.4		0	6.4	
Dox (ng/ml)	0	0	300	0	0	300
all data	4262	5131	5817	3245	3995	3817
usable data	4258	2746	3239	3242	0	0
lower quartile	44769	171743	179664	42188	-	-
median	54079	235900	244067	51660	-	-
upper quartile	62630	293967	299302	60686	-	-
IQR	17861	122223	119638	18498	-	-
minimum	19059	89408	89392	19775	-	-
maximum	89356	474389	472941	87281	-	-

Cell line	HCT 116/TK1tet cl.9					
FTD (μM)	0	6.4				
Dox (ng/ml)	0	0	10	30	100	300
all data	2611	2542	2414	2295	2431	2425
usable data	2604	4	32	197	812	1065
lower quartile	44013	85325	93386	124525	163856	206428
median	52835	85490	111675	210197	280886	303336
upper quartile	61065	85600	164557	317609	382829	391801
IQR	17051	275	71171	193084	218973	185373
minimum	20609	85075	86160	84814	84910	84867
maximum	84808	85682	243982	571356	708414	639776

Cell line	HCT 116/TK1tet cl.16					
FTD (μM)	0	6.4				
Dox (ng/ml)	0	0	10	30	100	300
all data	3432	3553	3515	3462	3346	2285
usable data	3411	8	81	474	1056	863
lower quartile	43176	82053	87248	138799	159392	168398
median	50885	83127	139099	245179	249001	247708
upper quartile	58651	83930	261412	357046	337297	344684
IQR	15476	1877	174163	218247	177905	176286
minimum	20329	81493	81477	81431	81533	81628
maximum	81404	85250	504021	677535	600956	607390

1.6. Figures

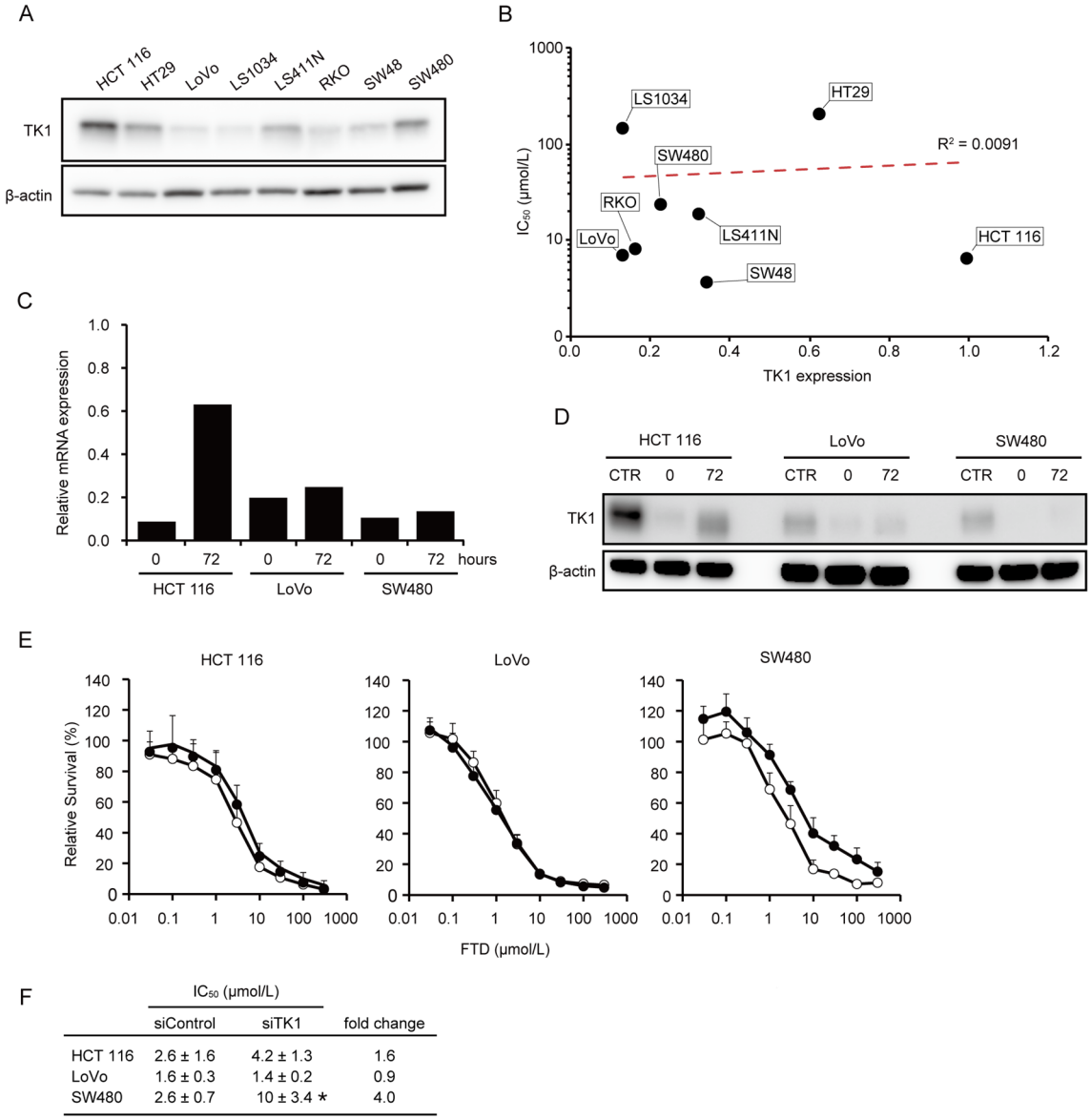

Figure 1-1: FTD Cytotoxicity in *TK1*-knock-down Colorectal Cancer Cells.

(A) Colorectal cancer cell lines were immunoblotted with the indicated antibody. (B) Correlation analysis between FTD cytotoxicity and the *TK1* expression level in A. (C, D) Cells were transfected with *TK1*-targeting siRNA. At 48 and 120 hours after transfection, which are indicated as 0 and 72 hours, respectively, cells were harvested and the mRNA (C) and protein (D) levels of TK1 were measured. (E) Influence of *TK1* knock-down on cytotoxicity of FTD. At 48 hours after transfection with control (open circles) or *TK1*-targeting (closed circles) siRNA, cells were treated with FTD for 72 hours and their viability was determined. All data are expressed as means ± SD. (F) Summary of the IC_{50} values in each cell line in (E).

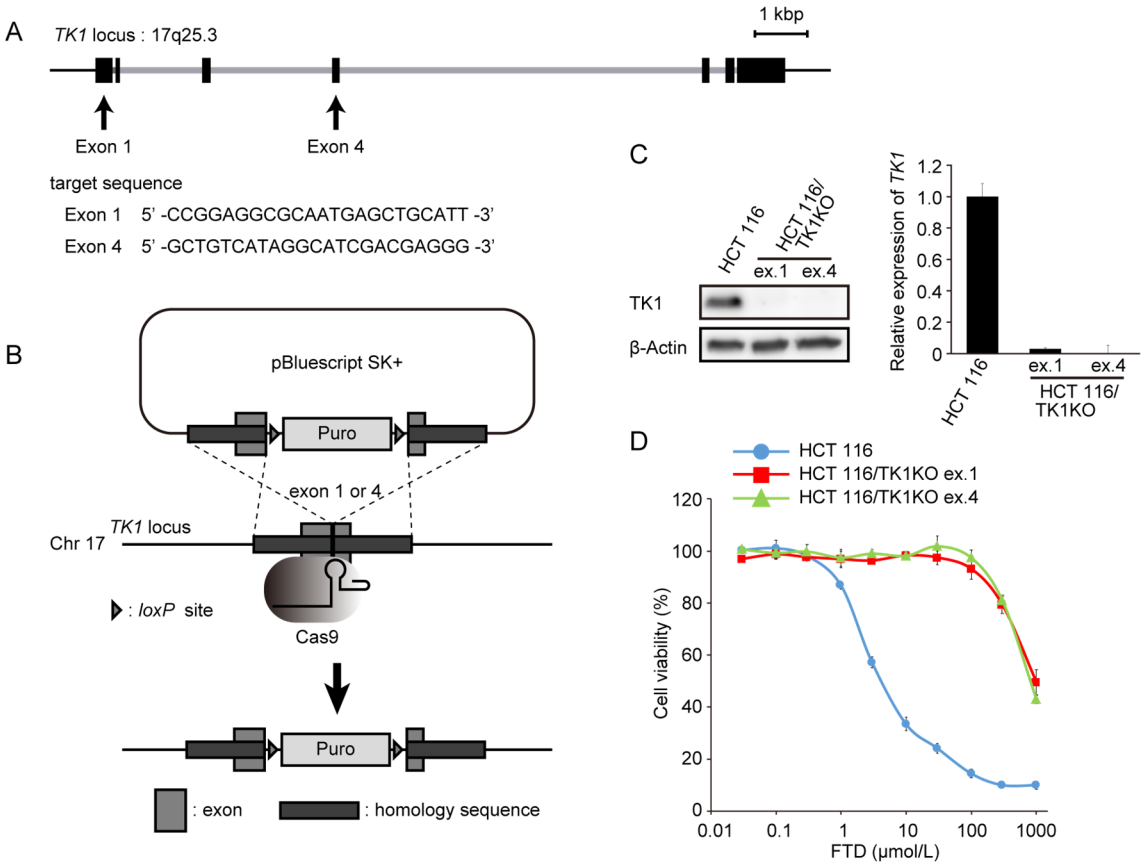

Figure 1-2: FTD Cytotoxicity in *TK1*-knock-out Cells.

(A) Schematic diagram of the *TK1* locus on Chr17q25.3. Exons are denoted by black rectangles and introns are shown in light grey. (B) Experimental scheme of *TK1* KO. Three PCR fragments, 600-700 base pairs of the right and left homology arms and a puromycin resistance cassette, were cloned into pBluescript SK+. (C) Western blot analysis of TK1 protein (left) and quantitative RT-PCR analysis of *TK1* mRNA (right) in HCT 116 parental and *TK1*-KO cells. Expression of *TK1* was normalized against that of *β-actin* and is plotted relative to that in HCT 116 parental cells. Data are means ± SD of three independent experiments. (D) Cell viability assay. Cells were treated with nine points of dilution series of FTD for 3 days and then their viability was determined. The viability of cells not treated with FTD was defined as 100%. Data are means ± SD of three independent experiments.

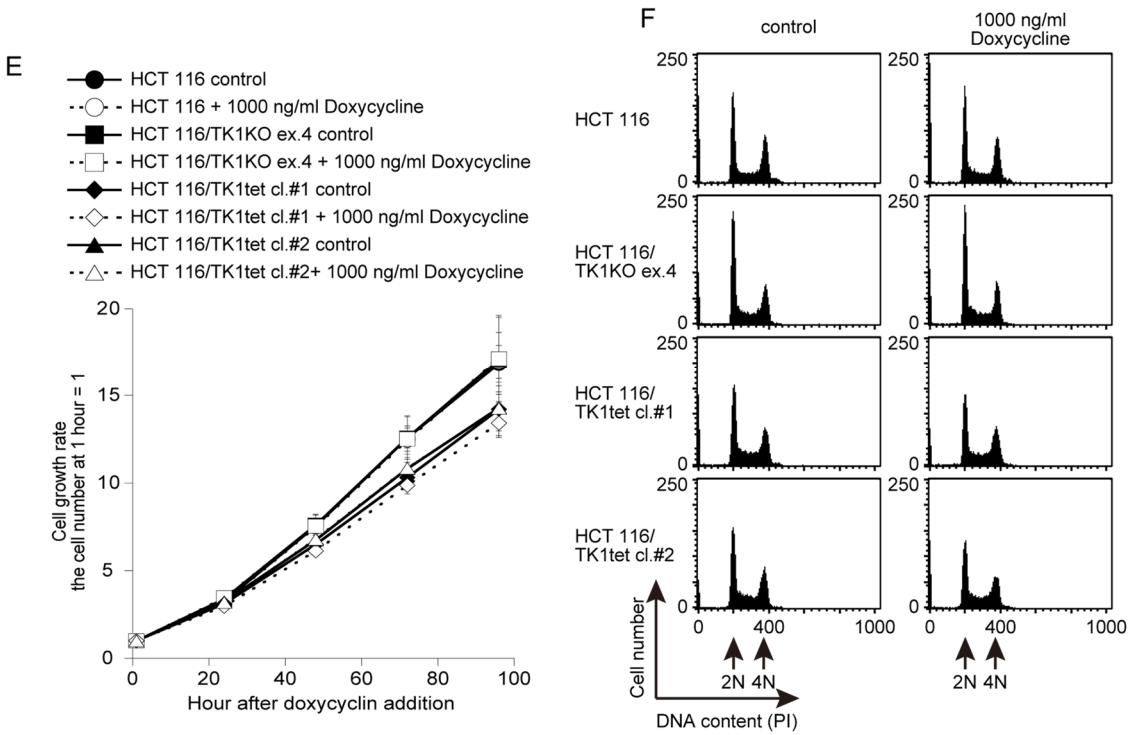

Figure 1-2: FTD Cytotoxicity in *TK1*-knock-out Cells. (Continued)

(E) Growth curve of each cell line treated with 0 or 1,000 ng/ml doxycycline. Cell viability was evaluated at 1, 24, 48, 72 and 96 hours after plating, and the cell growth rate relative to that at 1 hour was calculated. (F) Cell cycle distribution. Cells were treated with 0 or 1,000 ng/ml doxycycline for 1 day, fixed and stained with propidium iodide. The DNA content was quantitated using a FACSCalibur instrument.

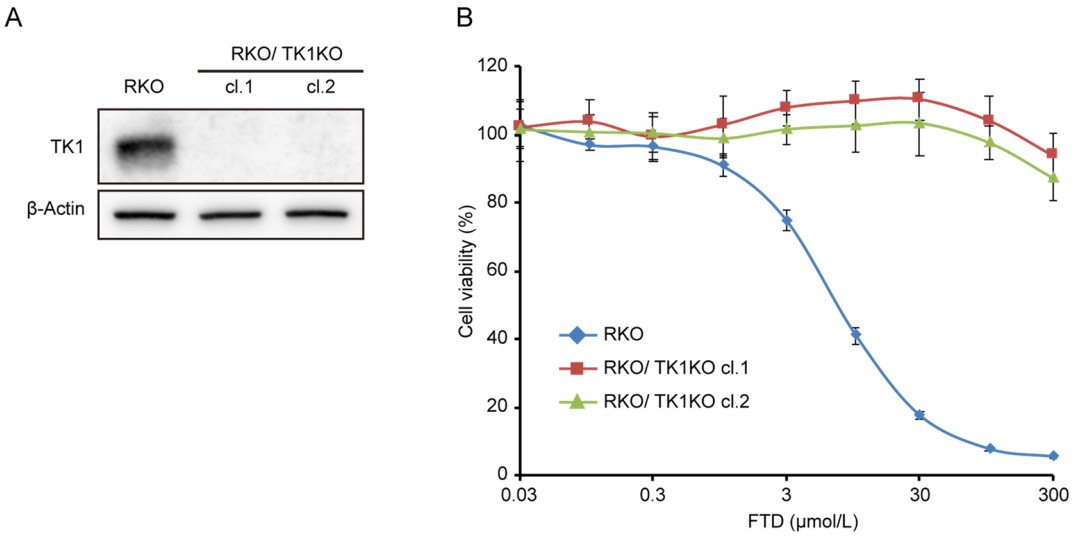

Figure 1-3: FTD Cytotoxicity in *TK1*-knock-out RKO Cells.

(A) Western blot analysis of TK1 protein in RKO parental and *TK1*-KO cells. (B) Cell viability assay. Cells were treated with nine points of dilution series of FTD for 3 days and then their viability was determined. The viability of cells not treated with FTD was defined as 100%. Data are means ± SD of three independent experiments.

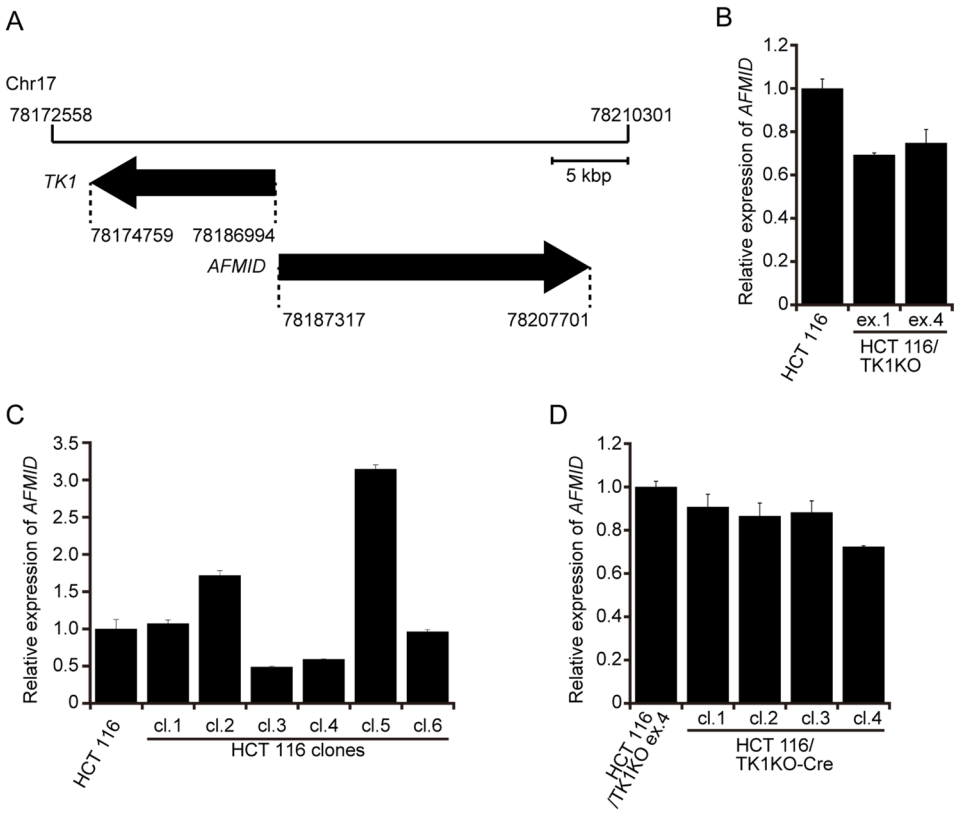

Figure 1-4: *AFMID* Expression in *TK1*-knock-out Cells.

(A) Schematic diagram around the *TK1* locus on Chr17. (B–D) Expression of *AFMID* was determined by quantitative RT-PCR, normalized against that of *β-actin* and plotted relative to that in HCT 116 cells. (B) *TK1*-KO cell lines. (C) Cloned HCT 116 cell lines. (D) The HCT 116/TK1KO ex.4 cell line and its clones whose puromycin resistance cassettes were removed by the Cre-*loxP* recombination system. Data are means ± SD of three independent experiments.

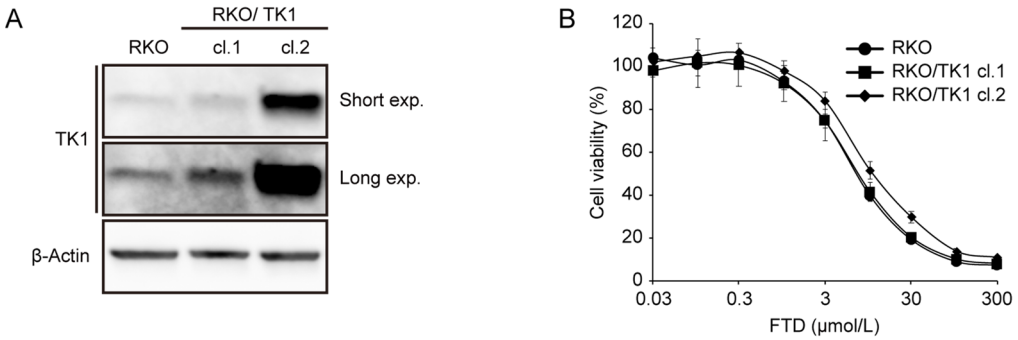

Figure 1-5: FTD Sensitivity of *TK1* Overexpressing RKO Cell Lines.

(A) Lysates of RKO cells stably expressing *TK1* were immunoblotted with the indicated antibodies. (B) Cells were treated with a dilution series of FTD comprising nine concentrations for 3 days and then their viability was determined. The viability of cells not treated with FTD was defined as 100%. Data are means ± SD of three independent experiments.

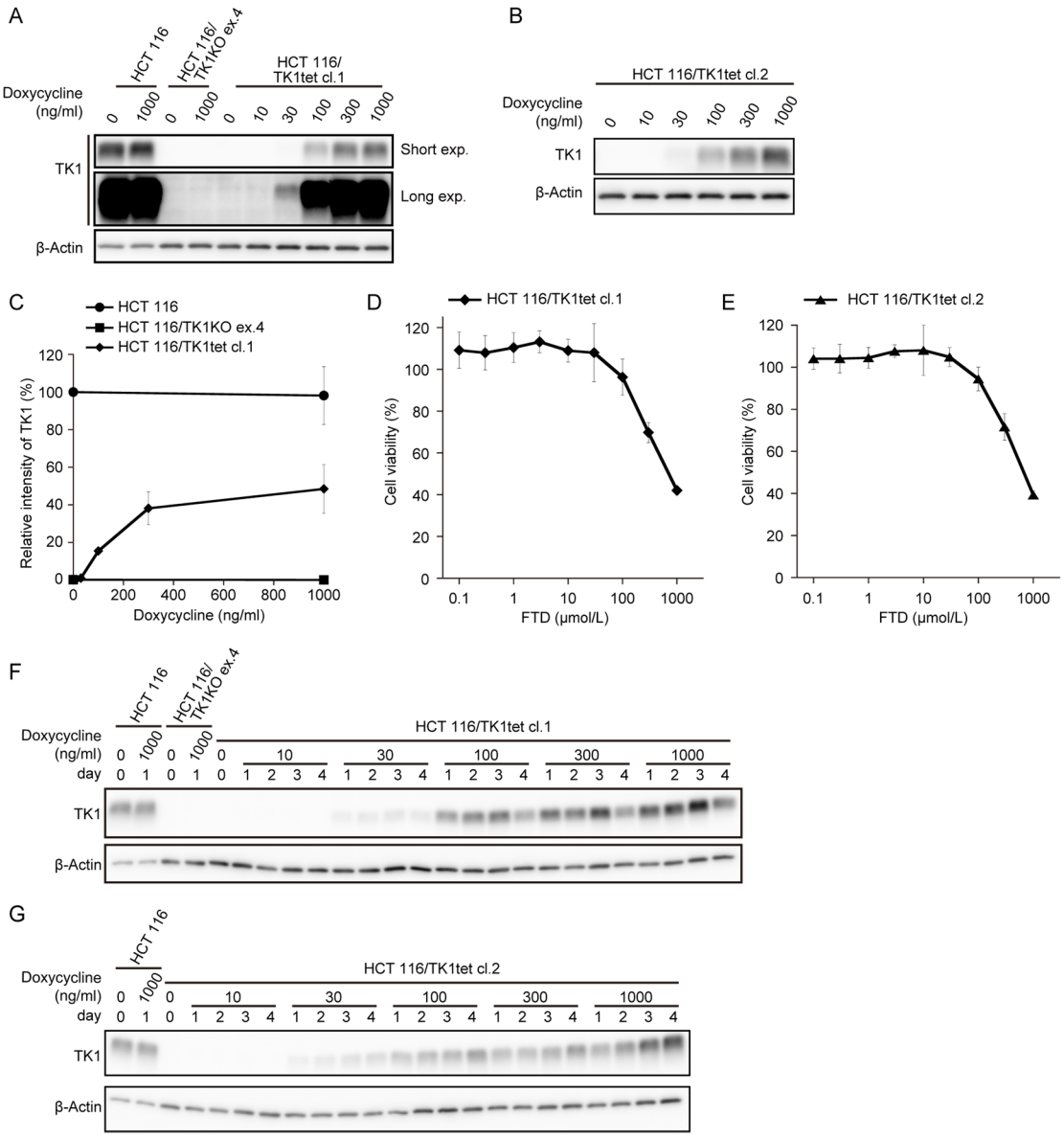

Figure 1-6: Correlation Between the TK1 Expression Level and FTD Incorporation or Cytotoxicity.

(A, B) Western blot analysis of TK1. HCT 116/TK1tet cl.1 (A) and cl.2 (B) cells were treated with the indicated concentration of doxycycline for 1 day and then the level of TK1 was analyzed. (C) Quantification of TK1 protein in (A). The intensity of the TK1 band was normalized against that of the β-actin band. The relative intensity of the TK1 band was calculated by setting that in cells not treated with doxycycline to 100%. Data are means ± SD of three independent experiments. (D, E) FTD sensitivity of HCT 116/TK1tet cl.1 (D) and cl.2 (E) cells. Cells were treated with the indicated concentration of FTD for 3 days and then their viability was evaluated. Relative cell viability was calculated by setting that of cells not treated with FTD to 100%. Data are means ± SD of three independent experiments. (F, G) Western blot analysis of TK1. HCT 116/TK1tet cl.1 (F) and cl.2 (G) cells were treated with the indicated concentration of doxycycline for the indicated number of days.

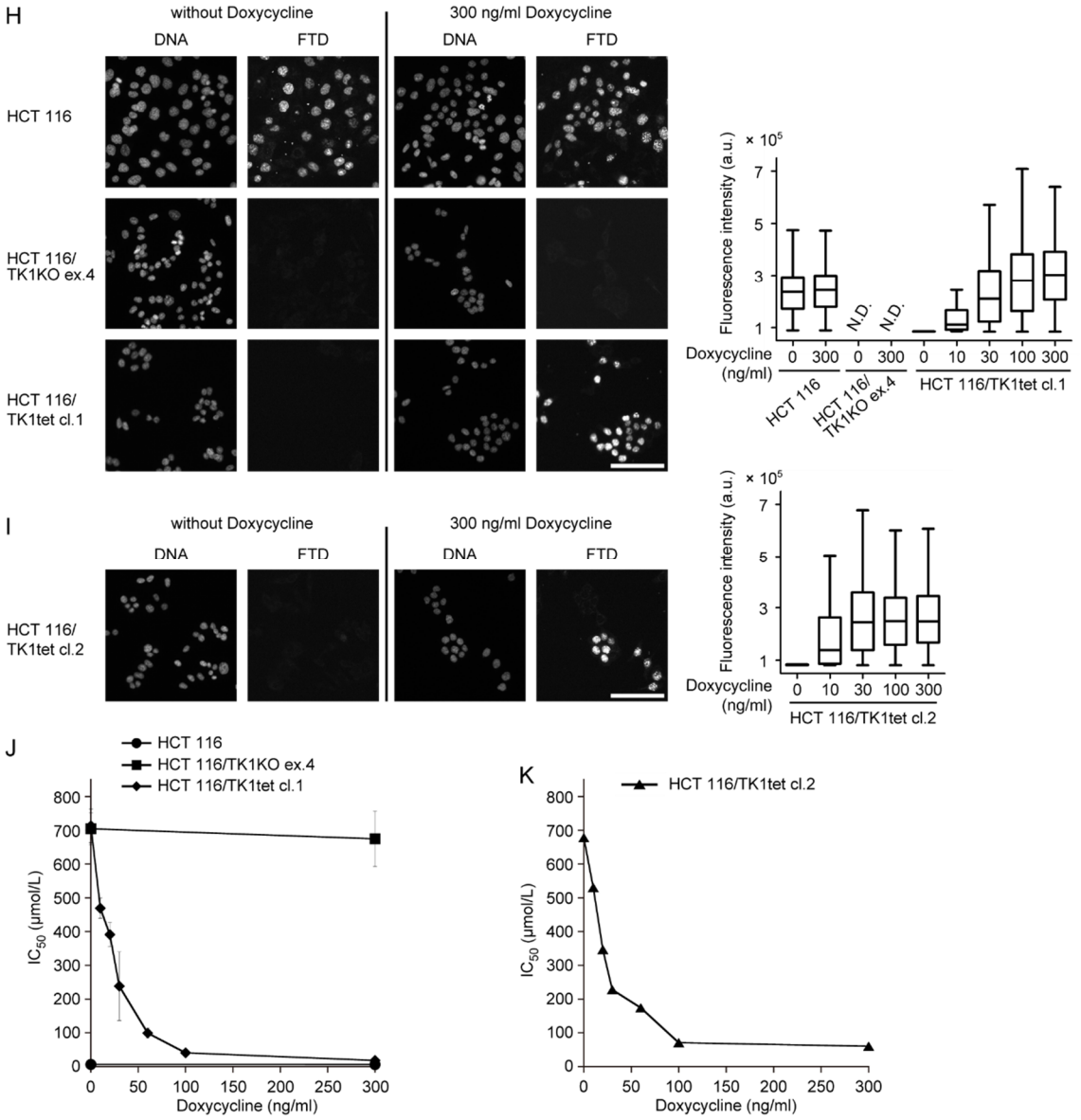

Figure 1-6: Correlation Between the TK1 Expression Level and FTD Incorporation or Cytotoxicity. (Continued)

(H, I) Immunofluorescence images of FTD-incorporated cells (left). Cells were treated with the indicated concentration of doxycycline for 1 day and then with 6.4 μmol/L FTD for 1 hour, fixed and immunostained with an anti-BrdU antibody. Fluorescence intensities of FTD incorporated into genomic DNA were quantified (right). Scale bar, 100 μm. (J, K) FTD sensitivity of HCT 116 parental cells, TK1-KO cells and HCT 116/TK1tet cl.1 (J), and HCT 116/TK1tet cl. 2 cells (K). Cells were treated with the indicated concentration of doxycycline for 1 day and then with nine points of dilution series of FTD for 3 days. The IC_{50} values in each cell line at the indicated concentration of doxycycline were calculated and plotted. Data are means ± SD of three independent experiments.

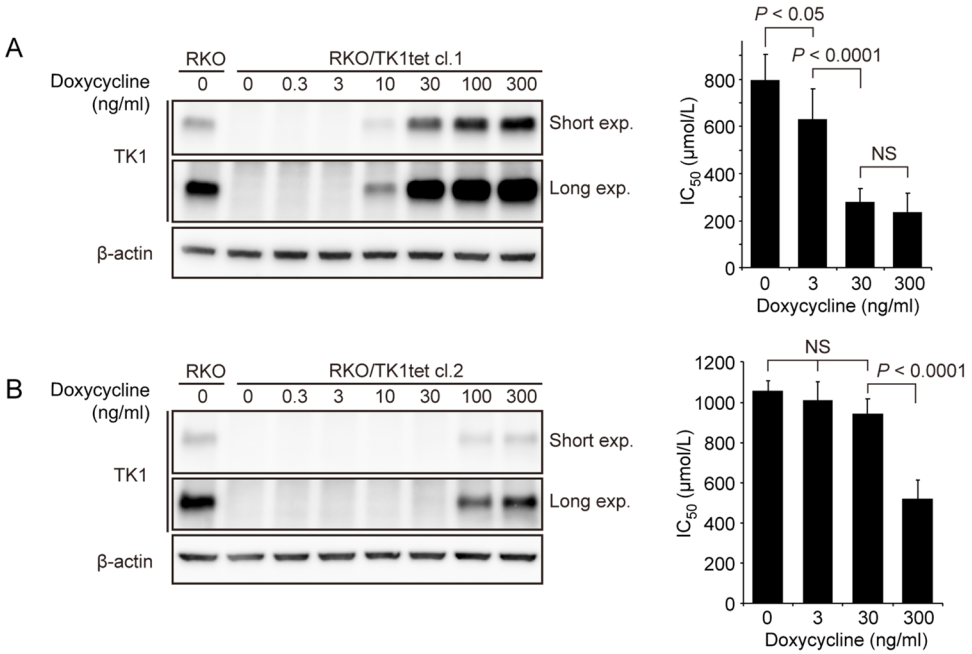

Figure 1-7: Response of RKO/TK1tet Cells to Doxycycline and FTC.

(A, B) Western blot analysis of TK1 (left) and FTD sensitivity (right). RKO/TK1tet cl.1 (A) and RKO/TK1tet cl.2 (B) cells were treated with the indicated concentration of doxycycline for 1 day and then the level of TK1 and IC_{50} values were analyzed. Data are means ± SD from six independent experiments. The p-values indicated in each panel were calculated by two-tailed *t*-test, NS, not significant.

2. Chapter 2: DNA Replication Stress Induced by Trifluridine Determines Tumor Cell Fate According to p53 Status

2.1. Introduction

Accurate DNA replication is fundamental to faithful genome duplication and cellular proliferation [34]. Obstacles that perturb DNA replication induce cellular stress termed DNA replication stress (DRS). Tumor cells often show dysregulation of DNA replication and sustained proliferation signaling, which leads to DNA damage and chronic DRS [35]. Conventional chemotherapy exerts cytotoxicity by causing DNA damage and simultaneously promotes DRS by perturbing DNA replication [3]. DRS induced by chemotherapy triggers the activation of cellular response pathways for survival in tumor cells; however, loss or suppression of the stress response can increase the susceptibility of tumor cells to catastrophic failure of proliferation. Thus, exploiting DRS is a feasible approach for cancer therapy [36].

DRS triggers various cellular responses in tumor cells. DRS activates ataxia telangiectasia and Rad3-related (ATR) kinase, which is recruited to replication protein A (RPA)-coated ssDNA at the stalled replication fork mediated by ATR-interacting protein (ATRIP) and it is slightly activated. In addition to ATRIP, many factors, such as RAD17, RAD9-RAD1-HUS1 (9-1-1) complexes, and TOPBP1 are indispensable for full activation of ATR. RAD17 is a clamp loader which loads the DNA clamp 9-1-1 complex on the stalled replication fork. Then RAD9, a component of 9-1-1 complex, is phosphorylated by slightly activated ATR. Furthermore TOPBP1 is recruited beside ATR by phosphorylated RAD9, and then ATR is fully activated by TOPBP1. The activated ATR transduces signals to Chk1, which is the main effector kinase, via phosphorylation to activate the S-phase checkpoint [37]. Thus, ATR and Chk1 preserve genome integrity by stabilizing the stalled fork and preventing origin firing. DRS also activates the Fanconi anemia (FA) pathway [38]. FA pathway activation, which is also ATR dependent [39, 40], results in FancD2 monoubiquitination, which plays a crucial role in stabilizing stalled replication forks [38]. In cases of moderate DRS, however, tumor cells proceeded to G_2 and M phases with under-replicated DNA (UR-DNA) at hard-to-replicate DNA regions, such as common fragile sites (CFS) [41]. The UR-DNAs formed ultrafine DNA bridges (UFB) at anaphase and induced genome instability phenotypes, such as lagging chromosomes and

micronuclei [42]. Moreover, chronic exposure to moderate DRS activates p53 and induces cellular senescence-like growth arrest [43]. Cellular senescence in tumor cells was also induced by anticancer chemotherapy and improved long-term outcomes [44].

Nucleoside analogue-type chemotherapeutic drugs, such as gemcitabine and cytarabine, are structurally similar antimetabolites with a broad range of action, and they are clinically active in both solid tumors and hematologic malignancies [45]. These drugs are efficiently transported into the cytoplasm of tumor cells, rapidly phosphorylated to triphosphate forms, incorporated into DNA during normal DNA synthesis by replicative DNA polymerases, and compromise DNA replication. FTD is a fluorinated thymidine analogue included in the clinically approved chemotherapeutic drug called FTD/TPI [7, 8]. FTD was extensively incorporated into DNA without detectable DNA strand breaks, induced Chk1 phosphorylation at serine 345 (pS345 Chk1), a specific site phosphorylated by ATR kinase upon DRS [37], and activated the p53-p21 pathway, leading to sustained cell-cycle arrest at a phase with 4N DNA content [12]. Although FTD induced cell death independently of p53 [46], the mechanism underlying the induction of DRS by FTD and its contribution to subsequent cell fate decisions remains to be fully elucidated.

In this study, I demonstrated that FTD delayed but did not terminate DNA replication *in vitro*. At the cellular level, FTD stalled replication forks and generated DNA lesions including single strand DNA, which persisted after S-phase was completed. In tumor cells, FTD led to the activation of the p53-p21 pathway, mitosis skipping, and persistent growth arrest characterized as cellular senescence. However, in p53-KO tumor cells, FTD led to aberrant mitosis with severely impaired sister chromatid separation, which caused apoptotic cell death. These data indicate that DRS induced by FTD treatment generated an antitumor effect by changing tumor cell fate according to the p53 status.

2.2. Materials and Methods

2.2.1. Cell Culture and Reagents

HCT 116 cells were purchased from ATCC in 2011. DLD-1 cells were provided by Taiho Pharmaceutical Co. Ltd. [20]. A549 cells were provided by Dr. M. Takeshita [12] (Kyushu University, Fukuoka, Japan). All cells were authenticated by short tandem repeat analysis (Biologica Co.) in 2018 and confirmed negative for Mycoplasma infection with the MycoAlert Mycoplasma Detection Kit (Lonza) in 2020. HCT 116 and A549 cells were cultured in DMEM, and DLD-1 cells were cultured in RPMI1640 supplemented with 10% FBS, 100 U/mL penicillin, and 100 μg/mL streptomycin at 37°C in 5% CO_2. Cells were stored in liquid nitrogen within two cell passages and the assays were performed on cells within 2 months after thawing. siRNA transfection was performed using RNAiMax reagent (Thermo Fisher Scientific). The siRNA sequences used were: *FancD2* (5′- GGAGAUUGAUGGUCUACUA -3′), and *Luc* (GL3: 5′ -CUUACGCUGAGUACUUCGA -3′). The following reagents were used: RO-3306, thymidine, chlorodeoxyuridine (CldU), iododeoxyuridine (IdU), bromodeoxyuridine (BrdU), dTTP, BrdUTP (Sigma-Aldrich), FTD (Tokyo Chemical Industry), and FTD triphosphate (FTD-TP) (Movarek Inc.).

2.2.2. DNA Fiber Analysis

DNA fiber analysis was performed as was described previously [47] with some modifications. For nascent DNA labeling, DLD-1 cells were cultured in the presence of 20 μmol/L CldU for 20 min, washed twice with fresh medium, and cultured in the presence of 20 μmol/L IdU or 20 μmol/L FTD for the indicated times. After double labeling, cell suspensions were spotted on slides, air-dried, and lysed with cell lysis solution (200 mmol/L Tris-HCl, pH7.5, 50 mmol/L EDTA, and 0.5% SDS). Following cell lysis, the slides were tilted to 15° to allow the DNA fibers to spread along the slides. After fixation with methanol/ acetic acid (3:1) and DNA denaturation with 2.5 N HCl, the DNA fibers on slides were immunostained with two different anti-BrdU antibodies (Supplementary Table 2-1), anti-mouse IgG conjugated with Alexa Fluor 568, and anti-rat IgG conjugated with Alexa Fluor 488 (Thermo Fisher Scientific) at 1:400 dilution. Slides were mounted with Vectashield (H-1000; Vector Laboratories).

2.2.3. *In vitro* DNA Polymerase Assay

The proteins used for the *in vitro* DNA polymerase assay (Fig. 2-2A) were purified as described previously [48-50]. Human DNA polymerase δ/ε activity was measured with reference to the incorporation of [α-^{32}P] dAMP. The reaction mixture (10 μL) contained 25 mmol/L HEPES-NaOH (pH 7.8), 0.1 mg/mL BSA, 0.5 mmol/L DTT, 10 mmol/L $Mg(CH_3COOH)_2$, 2 mmol/L ATP, 100 μmol/L each of dGTP, dCTP, dATP, the indicated concentrations of dTTP or dTTP analogue, 0.625–1.25 μmol/L [α-^{32}P] dATP, 12.4 fmol (90 pmol for nucleotides) of singly primed M13mp18 DNA (the 90-mer primer: 5′ -AGGCGGTCAGTATTAACACCGCCTGCAA CAGTGCCACGCTGAGAGCCAGCAGCAAATGAAAAATCTAAAGCATCACCTTGCTGA ACCTCA -3′ is complementary to nucleotide positions 4,833 and 4,922), 3.5 pmol replication protein A for Polδ or 3.5 pmol ssDNA binding protein for Polε, 1 pmol proliferating cell nuclear antigen (PCNA), 60 fmol replication factor C, and the indicated amounts of polymerase. After incubation at 37°C for 30 min, reaction mixtures were immediately chilled on ice, and 7 μL samples were spotted on Whatman DE81 paper (GE Healthcare). The unincorporated nucleotides were washed four times with 0.5 mol/L Na_2HPO_4, and the incorporated [α-^{32}P] dAMP adsorbed onto the paper was measured by Cherenkov counting using a liquid scintillation counter (Beckman Coulter).

To measure the DNA synthesis on the oligonucleotides, the 5′ end of the oligonucleotide primer was radiolabeled with [γ-^{32}P] ATP, annealed with the template oligonucleotide, and subjected to in vitro DNA polymerase reaction at 37°C for the indicated times. The reaction was stopped by adding a bromophenol blue/xylene cyanate-formamide EDTA solution. After boiling at 95°C for 3 min, the samples were loaded onto 15% acrylamide gels containing 7% urea and electrophoresed at 30 W for 60 min. The gels were fixed with 15% methanol/15% acetate solution for 10 min, rinsed with tap water, and dried on 3MM paper. Radioactivity was detected using BAS2000 (GE Healthcare).

2.2.4. Quantification of dTTP, FTD-TP, and BrdUTP Using LC/triplestage Quadrupole Mass Spectrometry

Intracellular dTTP, FTD-TP, and BrdUTP were quantified using LC-QqQ-MS (LCMS-8040; Shimadzu) as described previously [51]. FTD-TP and BrdUTP were detected with optimized selective reaction monitoring transitions in negative ionization mode as follows: FTDTP:

precursor ion [*m*/*z*] / product ion [*m*/*z*] = 535 / 159, 535 / 79, and 535 / 257 and BrdUTP: precursor ion [*m*/*z*] / product ion [m/z] = 546.5 / 159.

2.2.5. Generation of TP53-deficient HCT 116 Cells

First, a 20-mer sgRNA target sequence (5′- CTCAGAGGGGGCTCGACGCT -3′) at exon 2 of the TP53 gene was designed [18] and cloned into pX330 (Addgene #42230), which was a gift from Dr. Feng Zhang [19]. The donor DNA plasmid was constructed from the PCR fragment [~1,300-bp of the TP53 genomic region including the sgRNA target sequence amplified by PCR (forward: 5′ - ACTATATCCTTGTTAACAGGAGGTGGGAGC -3′ ; reverse: 5′ - AAGGGTGA AGAGGAATCCCAAAGTTCCAAAC -3′)] in pCR4-TOPO (Thermo Fisher Scientific), and its 130-bp BamHI fragment that includes the sgRNA target sequence was replaced with the 2,500-bp BamHI fragment containing a puromycin-resistant gene cassette [52]. The above two plasmids were cotransfected into HCT 116 cells using 4D Nucleofector (Lonza). The puromycin-resistant clones were screened by genomic PCR and sequencing.

2.2.6. Generation of Fluorescent Ubiquitination–based Cell-cycle Indicator-Expressing Cells by Lentiviral Infection

cDNA encoding mKO2-hCdt1 (aa 30–120) or mAG1-hGeminin (aa 1–110) amplified from the pFucci-G1 Red plasmid (AM-V9003) or pFucci-S/G2–M Green plasmid (AM-V9016; MBL), respectively, were cloned into the pENTR D-TOPO vector (Thermo Fisher Scientific). Each plasmid was mixed with pLenti6.4/R4R2/V5-DEST and pENTR 5′/EF1αP and recombined using LR Clonase II Plus enzyme (Thermo Fisher Scientific). The lentiviruses were produced using the ViraPower Lentiviral Expression System (Thermo Fisher Scientific). To establish HCT 116-fluorescent ubiquitination–based cell-cycle indicator (Fucci) or HCT 116 *p53*$^{-/-}$-Fucci cells, cells were infected with both lentiviruses encoding mKO2-hCdt1 (30–120) and mAG1-hGeminin (1–110) at a multiplicity of infection of 1 each. The infected cells were first selected by blasticidin (Thermo Fisher Scientific) treatment. The surviving cells were sorted in two steps using BD FACSAria SORP (BD Biosciences) as follows: cells emitting red fluorescence were sorted and cultured for several days, and the cells emitting green fluorescence were sorted.

2.2.7. Western Blot Analysis

Western blot analysis was performed, as was described previously [12]. The antibodies used are listed in Table 2-1. Chemiluminescence was detected using LAS 4000 mini (GE Healthcare).

2.2.8. Immunofluorescence

To visualize mitotic cells, cells were rinsed in PBS at 37°C, fixed in 4% paraformaldehyde (PFA) for 15 min at 37°C [53], permeabilized in PBS containing 0.1% Triton X-100 for 5 min at 37°C, and blocked in PBS containing 2% BSA for 30 min at room temperature. To visualize nuclear protein, cells were fixed with 3% PFA, 2% sucrose, and 0.5% Triton X-100 for 30 min on ice [54], permeabilized in PBS containing 0.1% NP-40, and blocked with PBS containing 3% BSA for 20 min at room temperature. To visualize FTD incorporated into DNA, cells were fixed with 70% ethanol, de-purinated with 1.5 N HCl, and blocked with PBS containing 5% goat serum, 0.3% Triton X-100 for 1 h at room temperature [23]. The cells were then incubated overnight at 4°C with the antibodies listed in Table 2-1. Secondary antibodies conjugated to Alexa Fluor 488, 568, or 647 (Thermo Fisher Scientific) were used. After washing in PBS containing DAPI for 5 min, cells were mounted on coverslips using ProLong Diamond or ProLong Glass (Thermo Fisher Scientific).

2.2.9. In Situ Proximal Ligation Assay

Cells were fixed in 3% PFA, 2% sucrose, and 0.5% Triton X-100 for 30 min on ice, permeabilized with PBS containing 0.25% Triton X-100 for 10 min at room temperature, blocked with PBS containing 3% BSA, and incubated overnight at 4°C with anti-FancD2 (NB100-182, Novus Biologicals) and anti-RPA32 (ab2175, Abcam) antibodies. PLA was performed with reagents from Duolink PLA technology according to the manufacturer's instructions (Sigma).

2.2.10. Image Acquisition

For fixed-cell experiments, fluorescence image acquisitions were performed using a Nikon A1R confocal imaging system or N-SIM super resolution imaging system controlled by NIS Elements software (Nikon). The objective lens was an oil immersion CFI SR ApoTIRF 100NA1.49 lens, an oil immersion Plan-Apo 100NA1.45 lens, or a Plan-Apo 40NA0.95 lens (Nikon). Images

were acquired as Z-stacks at 0.2-μm or 0.12-μm intervals with a confocal or a super-resolution microscope, respectively, and maximum-intensity projections were generated using the NIS Elements software (Nikon). The fluorescence intensity of RPA32 nuclear foci was quantified using Image J (NIH, Bethesda, MD) for each stack in the images with maximum-intensity projections. For live-cell imaging of cell-cycle progression, HCT 116-Fucci or HCT 116 *p53*$^{-/-}$-Fucci cells were imaged in a chambered coverglass (Matsunami) containing phenol red-free DMEM (Gibco). Live-cell imaging was performed, as was described previously [53]. The duration of the cell-cycle phases was calculated manually. For quantifying the nuclear foci and PLA signals, fluorescence images were acquired using a BZ-X800 (Keyence) with Plan-Apo 40 NA, and nuclear foci were counted using Hybrid Cell Count Software (Keyence). For quantifying the FTD incorporation into DNA, fluorescence images were acquired using a Cytell (GE Healthcare) and analyzed using In Cell Investigator software (GE Healthcare).

2.2.11. Animals and Evaluation of Antitumor Activity *in vivo*

All animal studies were performed according to the guidelines and with the approval of the institutional Animal Care and Use Committee of Taiho Pharmaceutical Co., Ltd. Ethical approval (March 5, 2019) was obtained prior to conducting the animal experiments. Male nude mice (CLEA Japan) were housed under specific pathogen-free conditions, with food and water provided *ad libitum*. The animals were quarantined for 1 week and then subcutaneously implanted with 1×10^7 HCT 116 or HCT 116 *p53*$^{-/-}$ cells on day 0. The mice were separated into each treatment group on day 3 so that the average body weight of each group was equivalent. FTD/TPI was prepared by mixing FTD and TPI at a molar ratio of 1:0.5 in 0.5% HPMC solution. FTD/TPI (FTD: 200 mg/kg/day) was administered orally twice daily from days 3–7, 10–14, and 17–21 at approximately 6 h intervals. For the control group, vehicle (0.5% HPMC solution) was administered at 10 mL/kg.

2.2.12. Statistical Analysis

The statistical analysis was performed using GraphPad Prism (GraphPad Software) or the EXSUS (CAC Croit Corp.) software. The Mann–Whitney *U* test was used in Figs. 2-1B, 2-4S, and 2-6C-F, the Kruskal–Wallis test in Figs. 2-4H, K, L, and Q, and the unpaired *t* test in Figs. 2-5L, 2-7B, and E.

2.3. Results

2.3.1. FTD Stalls Replication Forks and Activates the DNA Damage Response

FTD was found to induce pS345 Chk1, an indicator of the DNA damage response to DRS, during its misincorporation into DNA [12]. I hypothesized that FTD misincorporation itself would cause DRS and FTD-containing replication fork progression would be retarded. To evaluate the speed of individual active replication forks, I performed DNA fiber analysis [47]. Active elongating replication forks were labeled with CldU, and their elongation was measured by subsequent labeling with IdU or FTD (Fig. 2-1A, B) because IdU and FTD are recognized by B44 not by BU1/75 (Fig. 2-1C, D; [23]). FTD-containing forks were significantly shorter than IdU-containing replication forks (Fig. 2-1A, B). Furthermore, FTD, not CldU or IdU, induced pS345 Chk1 (Fig. 2-1E). These results indicate that FTD stalled replication forks during its incorporation into DNA and activated the DNA damage response.

2.3.2. FTD Impedes Replicative DNA Polymerases *In vitro*

I hypothesized that FTD triphosphate (FTD-TP) would be incorporated into DNA during replication, catalyzed by replicative DNA polymerases (Polδ and Polε) with low efficiency, which could slow the elongation of the nascent DNA strand. To test this possibility, DNA synthesis was evaluated by measuring the incorporation of radioactive [α-^{32}P] dATP in an *in vitro* reconstituted DNA replication assay using purified proteins (Fig. 2-2A-C). The [α-^{32}P] dATP incorporation rate was significantly lower in the presence of FTD-TP than in the presence of dTTP or BrdUTP (Fig. 2-2D). In addition, the low [α-^{32}P] dATP incorporation rate in the presence of FTD-TP was almost completely rescued when 50% of FTD-TP was replaced by dTTP (Fig. 2-2E). These results indicate that the incorporation rate of FTD-TP into the nascent DNA strand was less efficient than that of dTTP or BrdUTP.

To identify the specific sequence in the template DNA strand at which the synthesis of the nascent DNA strand is impeded in the presence of FTD-TP, I performed an *in vitro* DNA replication assay with a defined DNA template. The synthesis of the nascent DNA strand in the presence of FTD-TP was strongly and specifically impeded at positions of adenine-rich sequences (Fig. 2-2F).

I further examined whether the elongation of the nascent DNA strand was retarded when Polδ and Polε encounter FTD in the template DNA strand. Elongation was significantly suppressed

when either Polδ or Polε was used to replicate a template DNA strand containing five repetitive FTDs at the 3′ vicinity of the primer end (Fig. 2-2G). Collectively, these results indicated that FTD induced DRS by impeding the progression of replicative DNA polymerases during its incorporation into the nascent strand DNA, and also when FTD was present in the template DNA strand.

2.3.3. FTD Rapidly Decreases dTTP and Increases FTD-TP in the Cellular dNTP Pool

Next, I examined whether FTD-TP was produced when cells were cultured in the presence of FTD. In HCT 116 cells cultured in the presence of various concentrations of FTD for 60 min, FTD incorporation was detected (Fig. 2-3A) and dTTP decreased and FTD-TP increased in a concentration-dependent manner (Fig. 2-3B, C). In HCT 116 cells cultured in the presence of FTD, dTTP decreased rapidly as FTD-TP increased in the cellular dNTP pool (Fig. 2-3D, E). At this time point, FTD was being continuously incorporated into DNA (Fig. 2-3F) and induced pS345 Chk1 (Fig. 2-3G). When FTD was removed from the medium, dTTP recovered rapidly as FTD-TP disappeared from the dNTP pool (Fig. 2-3H, I). Furthermore, thymidine suppressed FTD incorporation into DNA in a concentration-dependent manner (Fig. 2-3J), and both thymidine and BrdU decreased FTD-TP and suppressed FTD-induced pS345 Chk1 (Fig. 2-3K-N). These data indicate that FTDTP was produced when cells were cultured in the presence of FTD and that it activated the DNA damage response during its incorporation into DNA.

2.3.4. FTD Induces FancD2 Monoubiquitination During S-phase and Results in the Accumulation of Persistent ssDNA

Next, I monitored cellular responses in synchronized HCT 116 cells cultured in the presence of FTD (Fig. 2-4A, B). FTD induced pS345 Chk1 and FancD2 mono-ubiquitination as cells proceeded through S-phase (Fig. 2-4C), indicating the activation of the ATR kinase and FA pathway in response to FTD. In contrast, FancD2 monoubiquitination was induced only minimally during S-phase in the absence of FTD (Fig. 2-4D-F). After completing S-phase, cells showed accumulation of p53 and p21 as they proceeded into the next cell-cycle phase with a 4N DNA content, which was accompanied by a decrease in the cyclin B1 level (Fig. 2-4C). Because nuclear retention and proteasome-mediated degradation of cyclin B1 occurs in a p53- and p21-dependent manner at G_2 phase when cells are permanently withdrawn from the cell cycle

[55], these data indicate that FTD activated p53-p21 pathway at G_2 phase as a consequence of DRS and enforced permanent exit from the cell cycle.

The accumulation of ssDNA is considered a hallmark of DRS and causes genome instability [56]. To investigate whether FTD treatment resulted in ssDNA accumulation, I coimmunostained the ssDNA binding protein RPA32 and FancD2 in FTD-treated HCT 116 cells. I observed a modest increase in the number of RPA32 nuclear foci at 24 h (Fig. 2-4G and H), when most cells were in S-phase (Fig. 2-4I). This was accompanied by pS345 Chk1 and FancD2 mono-ubiquitination (Fig. 2-4J) and the formation of pan-nuclear FancD2 foci (Fig. 2-4G, K). Intriguingly, the number of intense RPA32 nuclear foci were increased at 48 h (Fig. 2-4G, H), when most cells had a 4N DNA content (Fig. 2-4I), and p53 and p21 were induced (Fig. 2-4J). These data suggest that the FTD-treated cells accumulated ssDNA, which was associated with the replication fork stalling during S phase, and the ssDNA increased after cells completed the S-phase.

In human primary cells, FancD2 is required to restrain DNA synthesis under DRS and to prevent the accumulation of ssDNA and induction of p21 [57]. FancD2 and RPA32 were colocalized at FTD-induced nuclear foci (Fig. 2-4G). Furthermore, FTD increased significantly the number of PLA signals of FancD2 and RPA32 (Fig. 2-4L-N), confirming that FTD increased their association, bringing them into close proximity in the nucleus. I hypothesized that FancD2 would function near RPA-coated ssDNA after FTD treatment. To investigate this, I knocked down *FancD2* by siRNA, treated the cells with FTD (Fig. 2-4O, P), and evaluated the cellular responses induced by FTD. *FancD2* knockdown *per se* modestly increased the p21 level (Fig. 2-4O) but did not markedly affect FTD-induced p53-p21 activation (Fig. 2-4O), cell-cycle profile (Fig. 2-4P), or the number of FTD-induced RPA32 foci (Fig. 2-4Q). Intriguingly, *FancD2* knockdown significantly increased the intensity of each FTD-induced RPA32 focus (Fig. 2-4R, S), indicating that FancD2 suppressed the excess ssDNA accumulation induced by FTD.

2.3.5. FTD Induces Senescence in Tumor Cells with Wild-type p53 and Apoptosis in p53 Knockout Tumor Cells

FTD induced p53-dependent sustained cell-cycle arrest at the cell-cycle phase with a 4N DNA content [12]. To elucidate the role of p53 in the FTD-induced DNA damage response, I generated isogenic *TP53* gene KO HCT 116 cell lines with similar FTD sensitivity using the CRISPR/Cas9 system (Fig. 2-5A, B). In the presence of FTD, cell proliferation was similarly

suppressed in HCT 116 and HCT 116 *p53*$^{-/-}$ cells until day 3. In HCT 116 cells, proliferation ceased completely on day 6, and the cell number did not change until day 9. However, in HCT 116 *p53*$^{-/-}$ cells, the cell number started to decrease after day 3 and most cells had disappeared by day 9 (Fig. 2-5C). The same results were observed when FTD was removed from the cell culture media of both cell lines on day 3 (Fig. 2-5C), indicating that cell fate was determined before day 3.

I next examined the cellular response to FTD in HCT 116 and HCT 116 *p53*$^{-/-}$ cells (Fig. 2-5D). HCT 116 cells showed accumulation of p53 and p21 and almost undetectable expression of cyclin B1 and cyclin A proteins on day 3, at the time when accumulation of cyclin D1 was observed (Fig. 2-5D), suggesting that a significant proportion of cells were in the G_1 phase. In HCT 116 *p53*$^{-/-}$ cells, however, p21 and cyclin D1 did not accumulate, and cyclin B1 and cyclin A levels did not decrease (Fig. 2-5D). Furthermore, similar results were obtained using A549 (p53 wild-type) and DLD-1 (p53 mutant) cells (Fig. 2-5E-G). These data indicated that FTD activated the p53-p21 pathway and suppressed the growth of cells expressing wild-type p53, resulting in the accumulation of cells in G_1 phase, whereas in cells without p53, FTD caused tumor cell death.

Chronic DRS activated p53 and induced cellular senescence-like growth arrest [43]. Consistently, on day 3 of FTD treatment, most HCT 116 cells were senescence-associated β-galactosidase (SA-β-gal)-positive, whereas only a limited population of HCT 116 *p53*$^{-/-}$ cells showed this phenotype (Fig. 2-5H). Similar results were obtained with A549 and DLD-1 cells (Fig. 2-5I). Contrastingly, on day 6 of FTD treatment, the number of cells in the sub-G_1 population was greater in HCT 116 *p53*$^{-/-}$ cells than in HCT 116 cells (Fig. 2-5J). Immunoblot analysis showed a dramatic upregulation in markers of DNA damage (γH2AX) and apoptosis (cleaved PARP and caspase 3) in HCT 116 *p53*$^{-/-}$ cells but not in HCT 116 cells (Fig. 2-5D). These data indicate that cellular senescence and apoptotic cell death were predominantly induced in FTD-treated HCT 116 and HCT 116 *p53*$^{-/-}$ cells, respectively.

Finally, I examined the effect of tumor p53 status on the response to FTD/TPI treatment in an *in vivo* xenograft mouse model. FTD/TPI treatment significantly suppressed the growth of HCT 116 and HCT 116 *p53*$^{-/-}$ xenograft tumors (Fig. 2-5K, L), indicating that FTD/TPI exerts its tumor-suppressive effect irrespective of p53 status.

2.3.6. Cell Fate is Determined According to p53 Status at the G_2-M Transition Following an FTD-induced Extended S-G_2 Phase

I showed that FTD treatment determined cell fate in a p53-dependent manner. To explore this phenomenon in detail, time-lapse analysis of HCT 116 and HCT 116 *p53*$^{-/-}$ cells was performed using the Fucci system to visualize cell cycle status [58]. DNA damage-induced cellular senescence-like G_1-phase arrest proceeds via mitosis skip, which is a G_2-to-G_1-phase transition without mitotic cell division [1]. Consistent with this finding and the results of the SA-β-gal assay in HCT 116 cells (Fig. 2-5H), most HCT 116-Fucci cells showed a mitosis skip phenotype (Fig. 2-6A, second row, and B) after extending the duration of S-G_2 phase (Fig. 2-6C, D), whereas a minor proportion of HCT 116-Fucci cells displayed G_1-phase arrest after normal mitosis in response to FTD treatment (Fig. 2-6B). Furthermore, although HCT 116 *p53*$^{-/-}$ cells entered mitosis after extending the duration of S-G_2 phase (Fig. 2-6C, D), the duration of the second mitosis was severely extended (Fig. 2-6E, F), and cells exited mitosis and entered the next G_1 phase without separation into daughter cells, namely aberrant mitosis (Fig. 2-6A, fourth row, and B). Intriguingly, FTD treatment markedly extended the duration of the second S-G_2 phase rather than the first S-G_2 phase in both HCT 116 and HCT 116 *p53*$^{-/-}$ cells (Fig. 2-6C and D). Collectively, these data indicate that FTD treatment specifically slows the progression of S-G_2 phase irrespective of p53 status, although p53 is specifically involved in cell fate determination at the G_2-M-phase transition.

2.3.7. Severe Chromosomal Bridges are Induced by FTD During Late Mitosis in p53-null Cells

Upon mild perturbation of DNA replication, sister chromatids frequently interlinked at fragile sites, which are located at genetic loci with intrinsic replication difficulties, by BLM/PICH-associated UFBs [42]. I thus investigated whether FTD affects the formation of sister chromatid interlinks. First, to evaluate the effect of FTD treatment at the first S-G_2 phase on sister chromatid separation in the following anaphase, HCT 116 *p53*$^{-/-}$ cells were exposed to FTD in the presence of RO-3306, a Cdk1 inhibitor that perturbs the G_2-M-phase transition [59], and then released into mitosis in fresh medium for 50 min to enrich anaphase cells (Fig. 2-7A). Most anaphase cells showed separation of sister chromatids to the spindle poles; however, the appearance of PICH-associated UFBs, most of which also contained chromosomal bridges, was

also significantly increased (Fig. 2-7B). These results indicate that although FTD treatment-induced DRS during FTD-TP incorporation into nascent DNA strands partially disturbed the separation of several individual sister chromatids, it was not strong enough to prevent chromosome segregation.

Next, I observed anaphase chromosomes during the second mitosis in the presence of FTD, most of which incorporated FTD into the template DNA strand. HCT 116 *p53*$^{-/-}$ cells were exposed to FTD for 60 h, and chromosomal structures were observed in anaphase. To differentiate anaphase cells with unseparated sister chromatids from prometaphase cells, the cells were immunostained for cyclin B1, and only cyclin B1-negative cells that had already proceeded into anaphase were evaluated (Fig. 2-7C). Most anaphase cells showed no separation of sister chromatids to the spindle poles (Fig. 2-7D, E). In addition, super-resolution microscopy of centromere and microtubule staining showed that each kinetochore was captured by mitotic spindles (Fig. 2-7D, insets 4–6), similar to kinetochores with sister chromatids separated to the spindle poles as observed in normal anaphase cells (Fig. 2-7D, insets 1 and 2). Furthermore, a closer observation of each chromosome revealed that a significant population of sister chromatid pairs showed interlinking along chromosomal arms (Fig. 2-7D, inset 3), whereas the corresponding sister kinetochores were captured by spindles from the opposite spindle poles and were already separated (Fig. 2-7D, inset 4). These data indicate that, upon severe DRS induced by FTD treatment during the second S-phase, *p53*-KO cells displayed severe defects in sister chromatid separation at anaphase but not in the capture of kinetochores by spindles.

2.4. Discussion

In this study, I elucidated the mechanism underlying the antitumor effect of the fluorinated thymidine analogue-type chemotherapeutic drug, FTD. FTD treatment resulted in the replacement of dTTP in the dNTP pool with FTD-TP, which slowed DNA synthesis by replicative DNA polymerases. Thus, FTD stalled replication forks, activated ATR-dependent DNA damage responses, and resulted in the accumulation of RPA-coated ssDNA, which persisted even after cells completed the S-phase. FancD2 suppressed the FTD-induced ssDNA accumulation. Subsequently, FTD activated p53 and p21, thereby inducing cellular senescence. In the absence of p53, FTD triggered apoptotic cell death by inducing aberrant mitosis associated with severely unseparated sister chromatids. Because tumor cells show high levels of DRS and the cell survival depends on its response to DRS, exploiting DRS is a feasible approach for cancer therapy [36]. As a chemotherapeutic drug, FTD exploits cellular DRS and exerts antitumor effects irrespective of the p53 status of tumors (Fig. 2-8). In addition, tipiracil hydrochloride, as a component of FTD/TPI, inhibits thymidine phosphorylase and exerts an anti-angiogenesis effect [60], which may further enhance the cytotoxic effect of FTD.

Biochemical analysis of the *in vitro* reconstituted DNA replication using human Polδ and Polε revealed the unique properties of FTD as a nucleoside analogue. First, as a component of the dNTP pool, FTD-TP can replace dTTP during DNA synthesis at the replication fork; however, FTD-TP incorporation was inefficient. Another intriguing property of FTD-TP is that FTD incorporation did not terminate DNA polymerization, allowing its continuous incorporation into DNA to produce FTD-containing DNA strands. In contrast, other widely-used nucleoside analogue-type chemotherapeutic drugs, such as gemcitabine and cytarabine, terminated DNA polymerization in the vicinity of their incorporation in a cell-free system [45], strongly inhibited DNA synthesis at the cellular level [61], and were incorporated into DNA to a lower extent than FTD [10]. Second, as a component of the template DNA strand, FTD constitutes a continuous obstacle to DNA polymerization. This property may explain the severe extension of the second S-G_2 phase after FTD addition, because DNA synthesis at the second S-phase would have to proceed with the FTD-containing template DNA strand in the presence of FTD-TP in the dNTP pool. Third, FTD incorporated into the DNA of tumor cells was retained for a prolonged period [9]. This property would cause persistent disturbance of the replication process and a long-term tumor cytotoxicity, which may underlie the sustained growth-suppressive effect and

prolonged survival observed in a xenograft mouse model exposed to limited courses of FTD/TPI [10]. The dual perturbation of DNA replication caused by the inefficient incorporation of FTD during DNA synthesis and the persistent DNA polymerization roadblock caused by the presence of FTD on the template DNA strand are probably key properties of FTD.

Because FTD is a thymidine analogue, inefficient DNA replication should occur preferentially at the AT-rich genomic loci [62]. Recently, genome-wide analysis revealed that large homopolymeric dA/dT tracts were preferential sites of polar replication fork stalling and collapse within early-replicating fragile sites, CFSs, and replication fork barriers at ribosomal DNA [63]. FTD may exacerbate fork stalling at these fragile sites, retard S-phase progression, and increase ssDNA accumulation even after cells have completed the S phase. However, DNA strand breaks did not increase in FTD-treated HCT 116 cells [12]. FTD-induced ssDNA could be protected by the cooperative actions of proteins that accumulate in nuclear foci, such as FancD2 and the RPA complex. The RPA complex binds and stabilizes ssDNA [64] and FancD2 prevents excess ssDNA accumulation [57]. To repair or tolerate these abnormal DNA structures, homologous recombinational repair (BRCA1 or BRCA2), post-replicational repair (RAD18) and translesion DNA synthesis (REV3) may be involved, because vertebrate cells deficient in these factors showed higher FTD sensitivity [65]. Ultimately, the p53-p21 pathway was activated to avoid the catastrophic collapse of chromosomes [43]. On the other hand, in p53-KO cells, FTD induced ssDNA was probably converted to detrimental DNA strand breaks, as was evidenced by the detection of γH2AX, via aberrant mitosis progression and the failure of sister chromatid separation, probably caused by interlinks between ssDNA located at chromosomal arms.

Cell analysis revealed that FTD suppressed the growth of tumor cells irrespective of p53 status. This cellular outcome differed from that induced by gemcitabine, cytarabine, and fludarabine, which induced p53-dependent apoptotic cell death, and the loss of p53 conferred drug resistance [66]. The unique feature of FTD action is that it results in the p53-dependent divergence in cell fate at the G2-M-phase transition, resulting in the redirection of the cellular fate toward either senescence or apoptotic death. The p53-mediated senescence, however, impaired the apoptotic response to chemotherapy, and the senescent tumor cells showed persistent mitogenic potential, which caused relapse [67]. Recent studies indicate that the establishment of senescence may reprogram tumor cells into a latent stem-like state, resulting in tumor cells that escape senescence showing a more aggressive phenotype [68]. Because FTD is a component of the

chemotherapeutic drug FTD/TPI, whether FTD-induced senescent tumor cells also acquire stemness and a persistent mitogenic potential remains to be determined. If that is the case, a strategy for evading FTD-induced senescence or for directing tumor cell fate toward apoptotic death should be given serious consideration.

FTD/TPI shows efficacy in treating patients with gastrointestinal cancer who are refractory or intolerant of 5-FU-based therapy [7, 8]. At the cellular level, acquired resistance to 5-FU does not confer FTD resistance and vice versa [16, 20, 60, 69, 70], possibly reflecting the distinct mechanism of action of each drug. The unique property of FTD demonstrated in this study may also confer distinct cytotoxicity toward tumors that have acquired resistance to other conventional chemotherapeutic drugs. In addition, missense mutations, including both loss- and gain-of-function mutations, are frequently found in the TP53 gene locus of tumors obtained from patients [71]. Whether the expression of mutant p53 affects the cellular response and tumor cell fate decision induced by FTD is an important issue that warrants further investigation.

2.5. Table

Table 2-1: The List of Antibodies Used in This Study

Experiment	Antigen	Supplier	Cat#	Dilution
DNA fiber	BrdU (B44)	BD Bioscience	347580	1:25
	BrdU (BU1/75)	Abcam	ab6326	1:400
Western blot	β-actin	Sigma-Aldrich	A5316	1:10000
	Caspase 3	Cell Signaling Technology	9662	1:1000
	cleaved Caspase 3	Cell Signaling Technology	9664	1:1000
	Chk1	Santa Cruz Biotechnology	sc-8408	1:200
	phospho Ser345 Chk1	Cell Signaling Technology	2348	1:1000
	Cyclin A	Merk Millipore	05-373	1:500
	Cyclin B1	Merk Millipore	05-373	1:2000
	Cyclin D1	Santa Cruz Biotechnology	sc-20044	1:100
	FancD2	Novus Biologicals	NB 100-182	1:10000
	ɤH2AX	Merk Millipore	05-636	1:20000
	histon H3	Abcam	ab1791	1:2000
	PARP	Cell Signaling Technology	9542	1:2000
	Cleaved PARP	Cell Signaling Technology	5625	1:1000
	PCNA	Epitomics	2714-1	1:1000
	p53	DAKO	M7001	1:1000
	p21	Santa Cruz Biotechnology	sc-397	1:100
Immunofluorescence	α-tubulin	Sigma-Aldrich	T6199	1:2000
	BrdU (3D4)	BD Bioscience	555627	1:1000
	centromere (ACA)	Immunovision	HCT-0100	1:10000
	Cyclin B1	Merk Millipore	05-373	1:500
	FancD2	Novus	NB 100-182	1:500
	PICH	Merk Millipore	04-1540	1:50
	RPA32	Abcam	ab2175	1:200

2.6. Figures

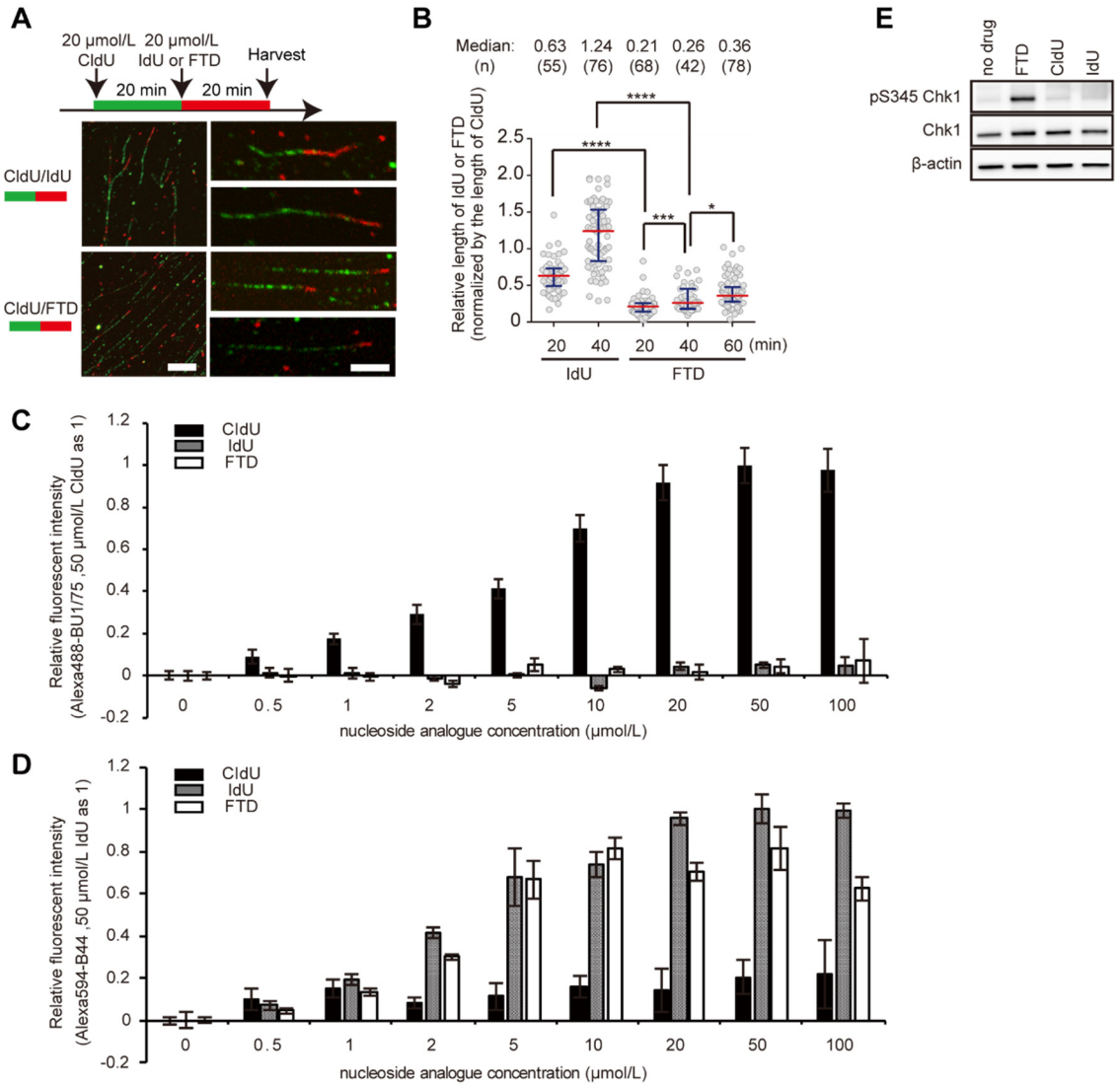

Figure 2-1: FTD Retards Replication Fork Progression.

(A) DNA fiber analysis; DLD-1 cells were cultured in the presence of 20 µmol/L CldU for 20 minutes and either of 20 µmol/L IdU (top) or 20 µmol/L FTD (bottom) for 20 minutes. Representative images are enlarged. Scale bars, 10 µm (left) and 5 µm (enlarged). (B) Scatter plot of relative IdU- or FTD-tract lengths normalized by the CldU-tract lengths for individual replication forks in A. Red lines denote median and blue whiskers extend to the quartiles. Mann–Whitney *U* test. (*, $P < 0.05$; ***, $P < 0.001$; ****, $P < 0.0001$). (C, D) Detection of nucleoside analogs by immunofluorescence staining. (C) Detection with the anti-BrdU antibody BU1/75. HCT 116 cells were cultured in the presence of CldU, IdU or FTD at the indicate concentrations for 1 hour and immunostained with the anti-BrdU antibody BU1/75. Relative fluorescence intensity was calculated considering the average amount of 50 µmol/L CldU as 1. (D) Detection with the anti-BrdU antibody B44. Relative fluorescence intensity was calculated considering the average amount of 50 µmol/L IdU as 1. (E) Western blot analysis; DLD-1 cells were cultured in the presence of 20 µmol/L nucleoside analogues for 1 hour.

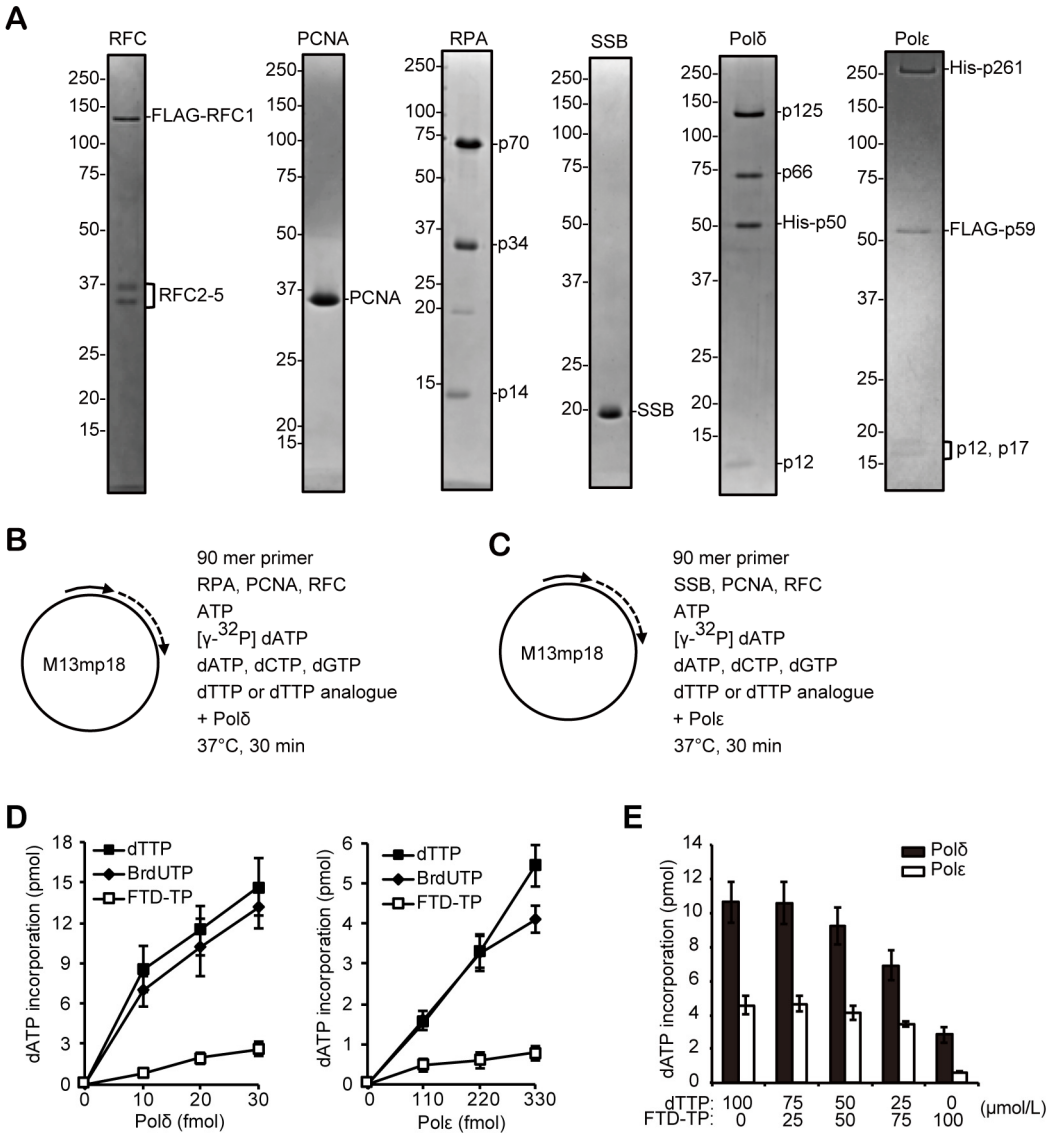

Figure 2-2: FTD Reduces DNA Replication Efficacy.

(A-C) Experiment design of the *in vitro* DNA synthesis assay. (A) Purified proteins. Coomassie blue staining of each purified protein or protein complex is shown. The protein purification methods are described in Materials and methods. (B) Schematic of the *in vitro* DNA synthesis assay using Polδ. (C) Schematic of the *in vitro* DNA synthesis assay using Polε. (D) The *in vitro* DNA synthesis rate of replicative polymerases Polδ (left) and Polε (right), in the presence of dTTP, BrdUTP, or FTD-TP. DNA synthesis was measured by [α-32P] dATP incorporation into the nascent strand DNA using M13mp18 ssDNA plasmid as a template. Error bars, SD of three independent experiments. (E) Relative *in vitro* DNA synthesis rates in the presence of the dTTP/FTD-TP mixture. Error bars, SD of three independent experiments.

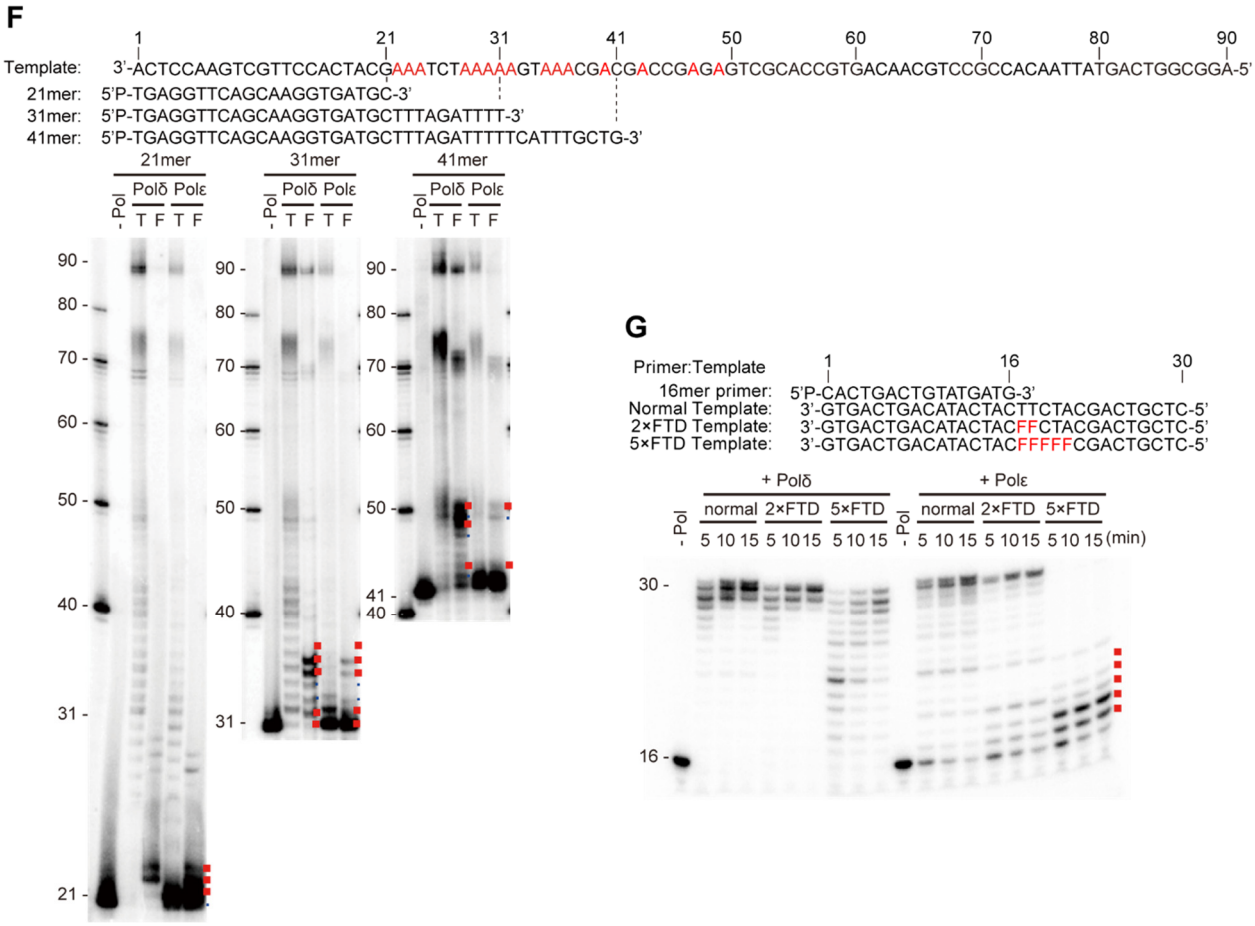

Figure 2-2: FTD Reduces DNA Replication Efficacy. (Continued)

(F) The *in vitro* DNA synthesis of Polδ and Polε in the presence of FTD-TP. Sequences of 5′-radiolabeled primers (21-mer, 31-mer or 41-mer) and template 90-mer oligonucleotides of the *in vitro* DNA synthesis analysis are shown on top. Adenine sequences in the template oligonucleotide are marked by red. DNA synthesis from radiolabeled primers of the 90-mer oligonucleotide template is shown on the bottom. The DNA synthesis reaction catalyzed by Polδ and Polε was performed in the presence of dTTP (T) or FTD-TP (F). Reaction in the absence of replicative polymerase is shown by −Pol. The bands representing DNA synthesis stopped at adenine sequences are marked by red dots. (G) The *in vitro* DNA synthesis catalyzed by Polδ and Polε from a DNA template containing FTD. Sequences of the 5′-radiolabeled 16-mer primer and template 31-mer oligonucleotides (Normal, 2×FTD, 5×FTD template) of the *in vitro* DNA synthesis analysis are shown on the top and repetitive FTD (F) sequences in the template oligonucleotide are marked by red. DNA synthesis from radiolabeled primers of the 31-mer oligonucleotide template is shown on the bottom. The DNA synthesis reaction catalyzed by Polδ and Polε was performed for the indicated times (min). Reaction in the absence of replicative polymerase is shown by –Pol.

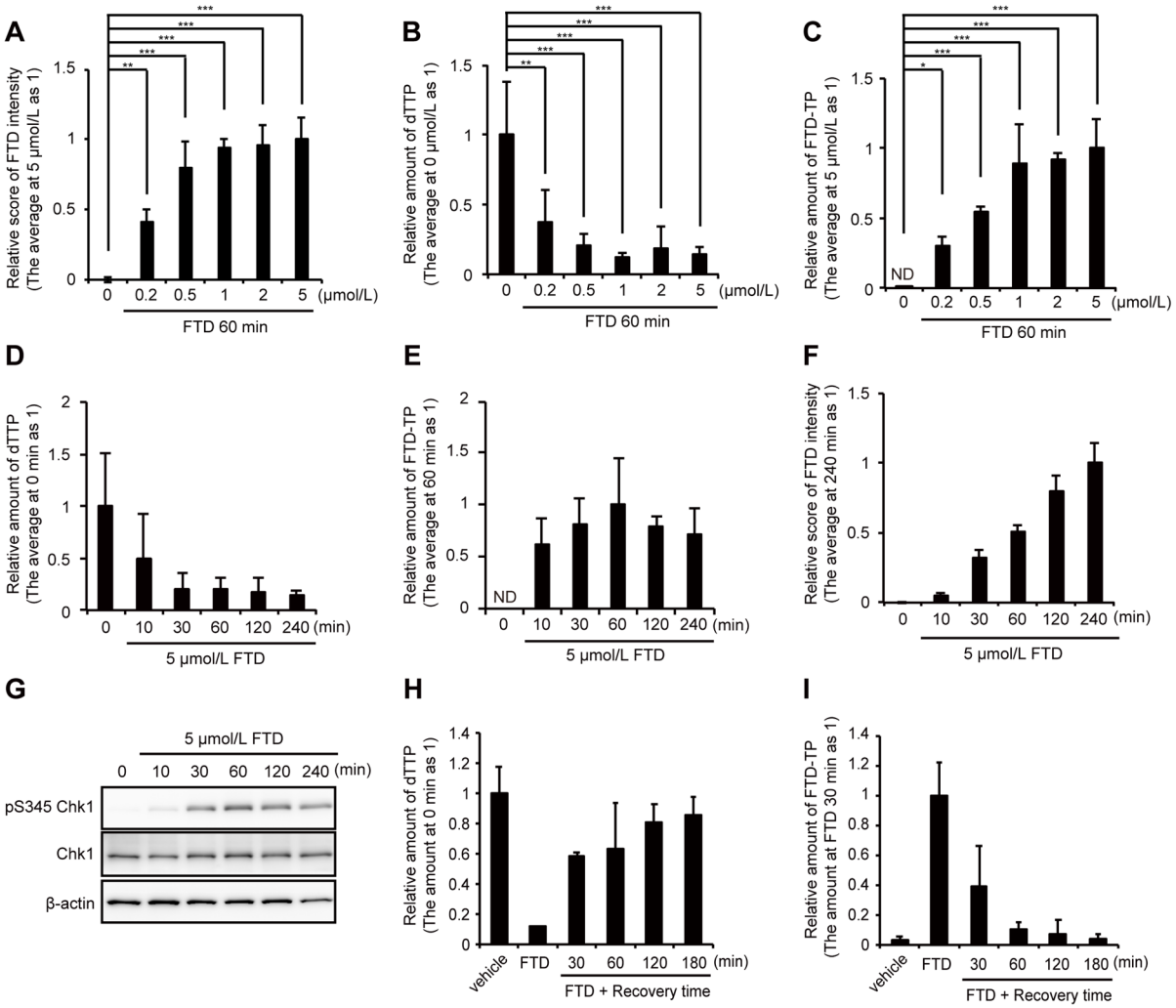

Figure 2-3: Effect of FTD on the Cellular and Metabolomic States.

(A-C) Effect of various concentration of FTD on the cellular and metabolomics states. (A) FTD incorporation into DNA. The relative fluorescence intensity was calculated considering the average amount of 5 μM FTD as 1. Relative amount of cellular dTTP (B) and FTD-TP (C). The relative scores were calculated considering the average amount of 0 μmol/L FTD (B) or 5 μmol/L FTD (C) as 1. (A-C) Williams' multiple comparison test. (*, $P < 0.025$; **, $P < 0.005$; ***, $P < 0.0005$). (D-I) Effect of 5 μmol/L of FTD on the cellular and metabolomics states. Relative amounts of cellular dTTP (D) and FTD-TP (E). The relative scores were calculated by considering the average amount at 0 minutes (D, 70.6 ± 31.3 pmol/10^6 HCT 116 cells, n = 3) or 60 minutes (E, 57.7 ± 47.1 pmol/10^6 HCT 116 cells, n = 3) of 5 μmol/L FTD treatment as 1, respectively. ND: not detectable. (F) FTD incorporation into DNA. The relative scores were calculated by considering the average amount at 240 minutes of 5 μmol/L FTD treatment as 1. (G) Western blot analysis; HCT 116 cells were cultured in the presence of 5 μmol/L FTD and harvested at the indicated time points. pS345 Chk1, Chk1 phosphorylation at Ser345. Relative amounts of cellular dTTP (H) and FTD-TP (I) after the change to drug-free media. The relative scores were calculated by considering the average amount at 0 minutes (H) or 5 μmol/L FTD 30 minutes (I) as 1, respectively. Error bars, SD of three independent experiments.

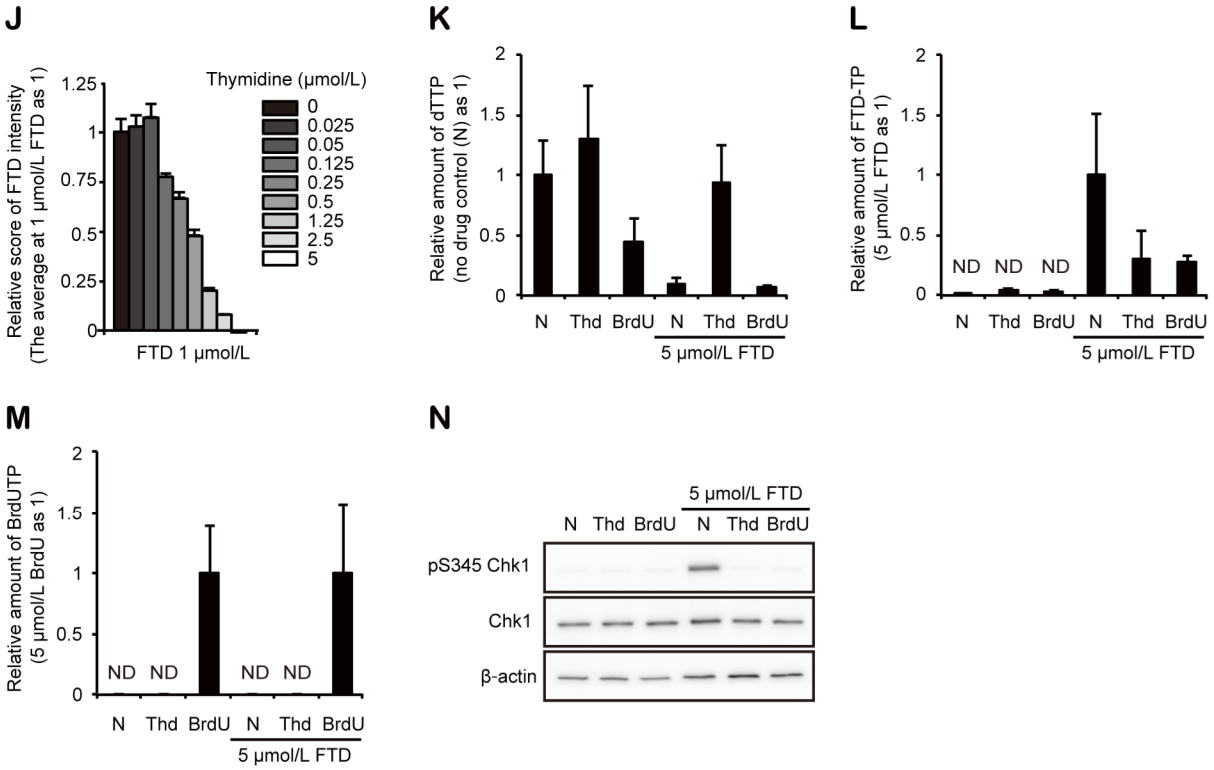

Figure 2-3: Effect of FTD on the Cellular and Metabolomic States. (Continued)

(J) The suppression of FTD incorporation into DNA by thymidine. HCT 116 cells were cultured 1 hour in the presence of 1 μmol/L FTD with various concentration of thymidine. FTD was immunostained with anti –BrdU antibody (3D4). (K-N) Effect of thymidine and BrdU on FTD-induced metabolomics states and DNA damage response. Relative amount of 0 μmol/L FTD (K), 5 μmol/L FTD (L), or 5 μmol/L BrdU (M) as 1. (N) Western blot; pS345 Chk1: Chk1 phosphorylation at Ser345.

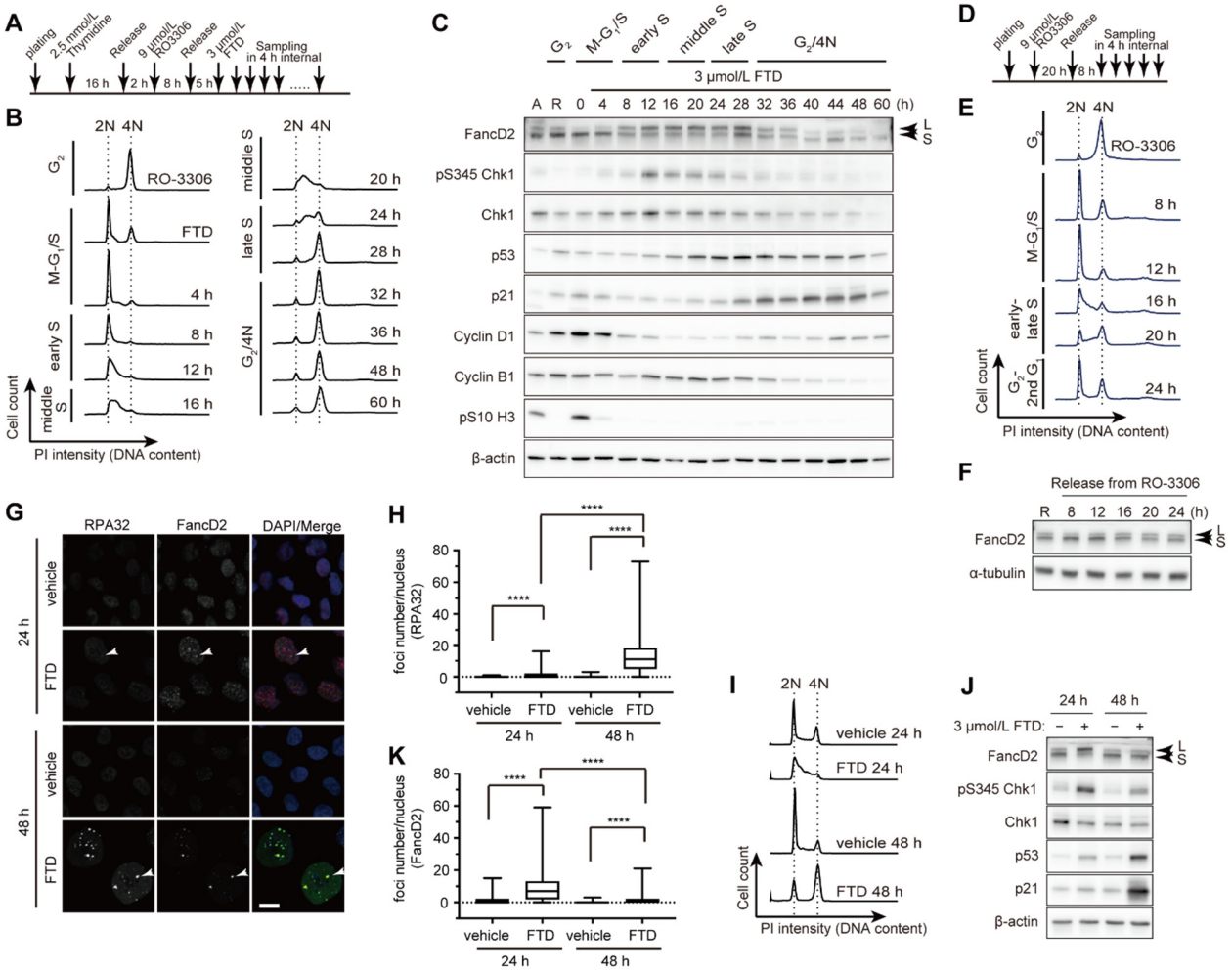

Figure 2-4: DNA Damage Response to FTD in HCT 116 Cells.

(A) Schedule of thymidine-RO-3306 synchronization. (B) Histograms of samples in (A). HCT 116 cells with thymidine-RO-3306 synchronization were released and cultured in the presence of 3 μmol/L FTD. The position of cells with 2N and 4N DNA content are indicated by dashed lines. (C) Western blot; DNA damage response of synchronized HCT 116 cells. A, Asynchronous; R, RO-3306 arrested. Cell-cycle phases at each time point are indicated above. (D) Schedule of RO-3306 synchronization. (E) Histograms of samples in (D). (F) Western blot of samples shown in (D). (G) Immunofluorescence images of FancD2 and RPA32 in HCT 116 cells, which were cultured in the presence of 3 μmol/L FTD for indicated time. Representative colocalizing foci are indicated by arrows; scale bar, 10 μm. Box plots of the number of RPA32 foci (H), and FancD2 foci (K) in (G). Kruskal–Wallis test. (****, $P < 0.0001$). (I) Histograms of samples shown in (D, H, K, and L). (J) Western blot samples shown in (D, H, I, K, and L). L and S indicate large (monoubiquitinated) and small (non-ubiquitinated) isoforms of FancD2.

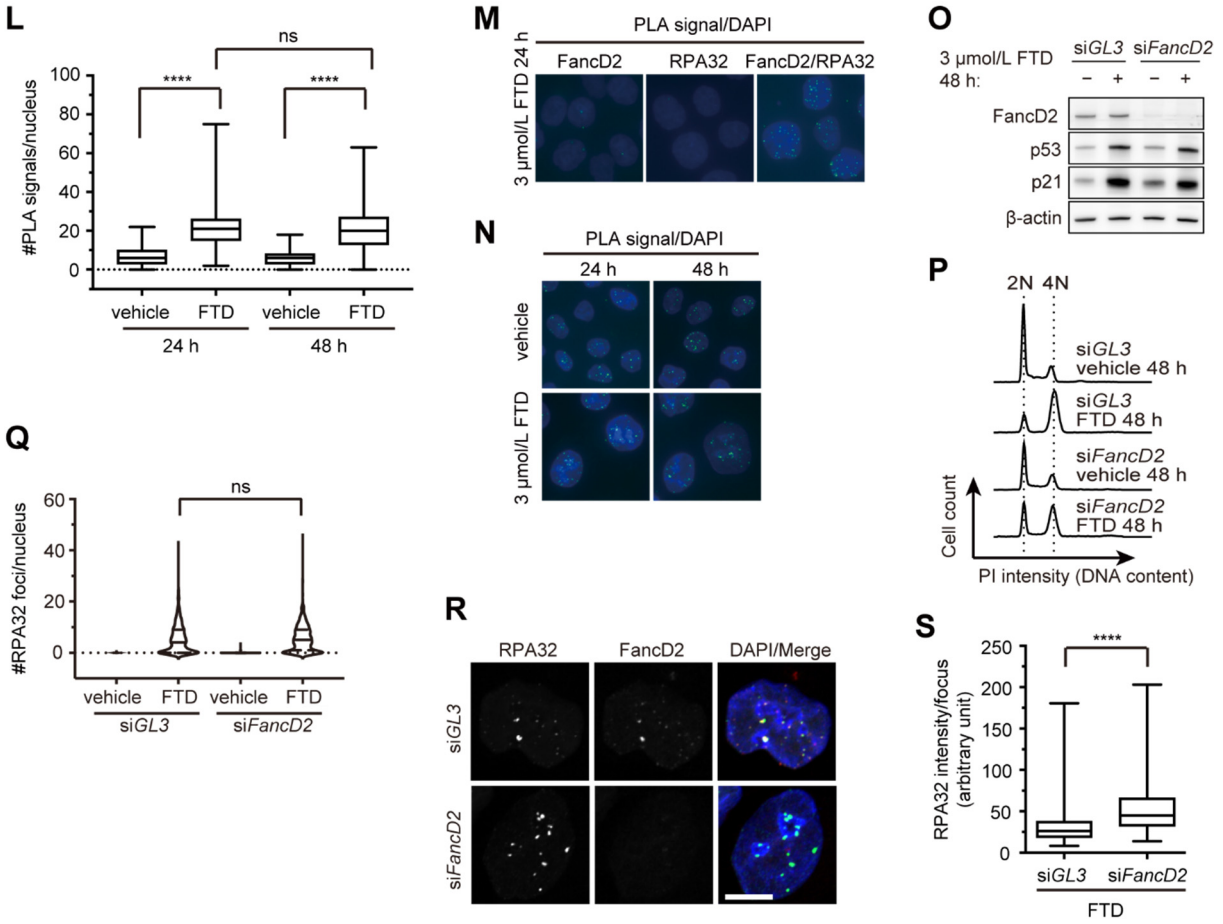

Figure 2-4: DNA Damage Response to FTD in HCT 116 Cells. (Continued)

(L) Box plots of the number of proximal ligation assay (PLA) signals between FancD2 and RPA32 per each nucleus of HCT 116 cells, which were cultured in the presence of 3 μmol/L FTD for indicated time. Two hundred nuclei for each time point were counted in three independent experiments. The horizontal lines indicate medians, and the boxes and whiskers indicate the interquartile and minimum/maximum ranges, respectively. Kruskal–Wallis test. (****, $P < 0.0001$; ns, not significant). (M) PLA signals with anti-FancD2 only, anti-RPA32 only, and anti-FancD2 and anti-RPA32 together. (N) Representative images of PLA signals of anti-FancD2 and anti-RPA32. Quantitative data are shown in (L) (O) Western blot of si*FancD2*- and FTD-treated HCT 116 cells. (P) Histogram of samples shown in (O, R, and S) (Q) Violin plots; the number of RPA32 foci per each nucleus of si*FancD2*- and FTD-treated HCT 116 cells was plotted. Two hundred nuclei for each time point were counted in three independent experiments. The horizontal solid and dashed lines indicate the median and the quartiles, respectively. Kruskal–Wallis test. ns: not significant. (R) Immunofluorescence images of FancD2 and RPA32 in siFancD2- and FTD-treated HCT 116 cells, which were cultured in the presence of 3 μmol/L FTD 48 hours; scale bar, 10 μm. (S) Box plots of the intensity of each RPA32 focus in (R). The integrated intensity of each focus was plotted. Two-hundred foci were measured in three independent experiments. The horizontal lines indicate medians, and the boxes and whiskers indicate the interquartile and minimum/maximum ranges, respectively. Mann–Whitney *U* test. (****, $P < 0.0001$).

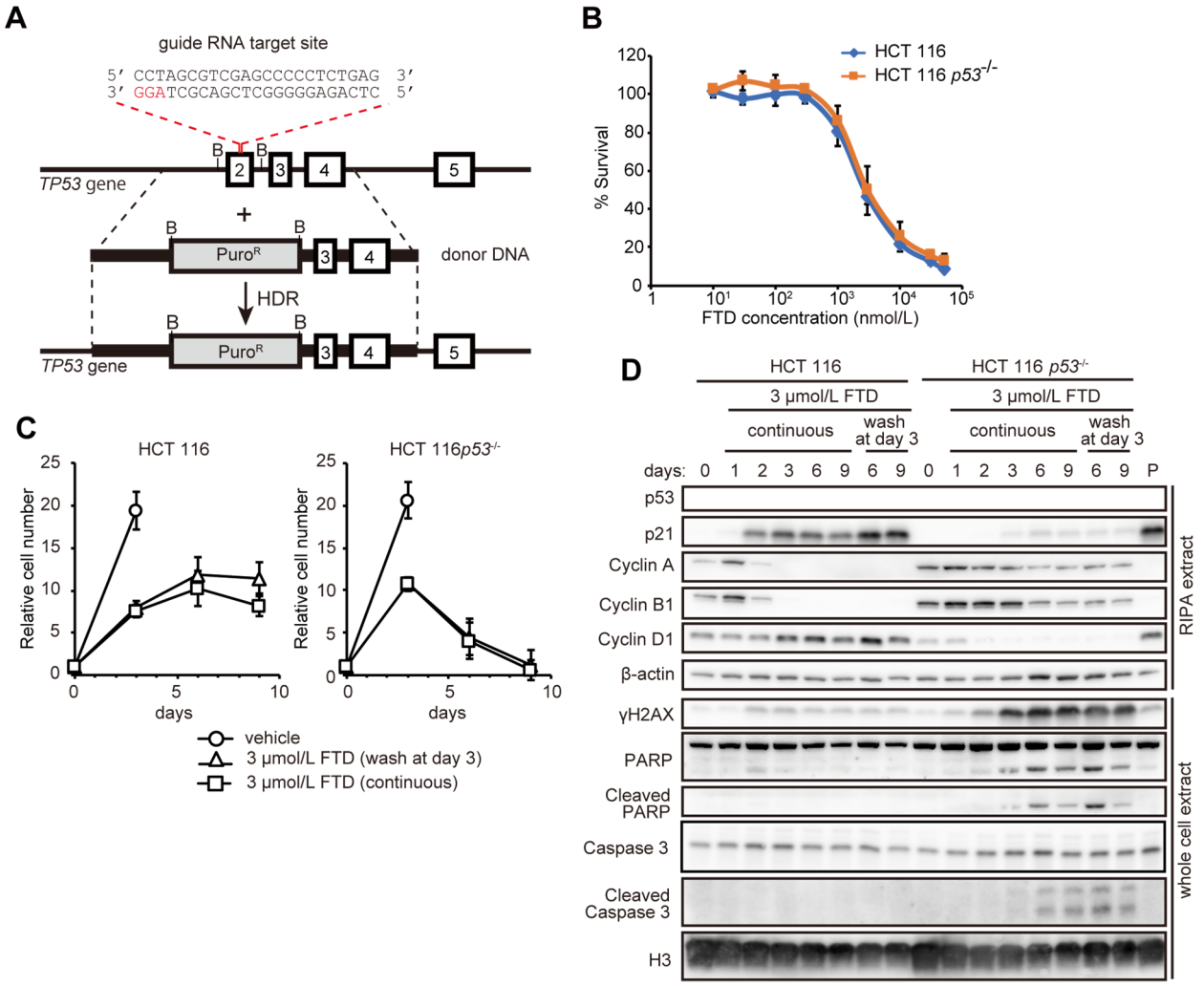

Figure 2-5: Outcomes of Cells Cultured in the Presence of FTD.

(A, B) Gene targeting of the TP53 gene by CRISPR/Cas9. (A) Schematic design of CRISPR/Cas9-mediated gene targeting. The position and sequence of the guide RNA, donor DNA, and the targeted allele are shown. B indicates the BamHI site. (B) Viability of HCT 116 and HCT 116 *p53*$^{-/-}$ cells in the presence of various concentrations of FTD on day 3. (C) Growth curve; cell growth was measured by crystal violet staining on the indicated days. Error bars represent SD of three independent experiments. (D) Western blot analysis; HCT 116 and HCT 116 *p53*$^{-/-}$ cells were cultured in the presence of 3 µmol/L FTD either continuously (continuous) or for 3 days (wash at day 3) for the indicated days and harvested. P represents a positive control (HCT 116 cells, which were cultured in the presence of 3 µmol/L FTD for 3 days).

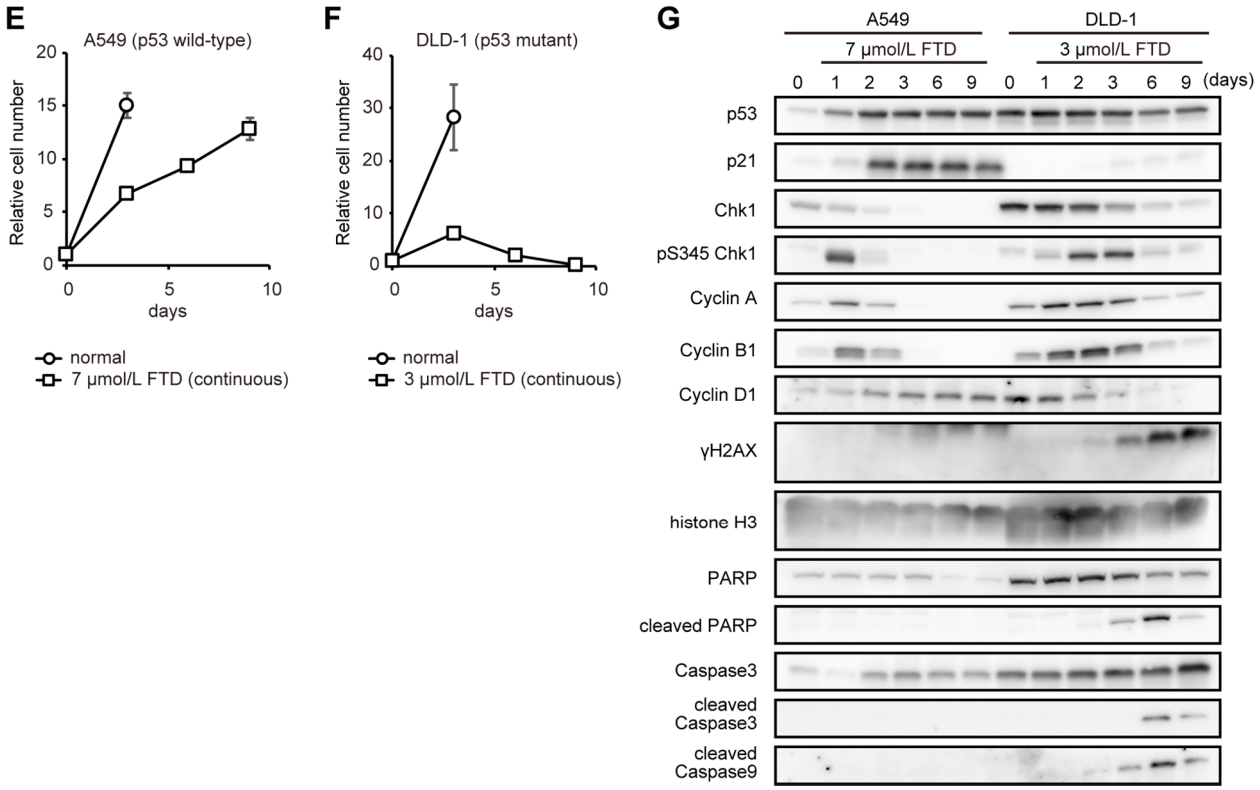

Figure 2-5: Outcomes of Cells Cultured in the Presence of FTD. (Continued)

Cellular responses of A549 and DLD-1 cells. Proliferation rate (A549: E, DLD-1: F), DNA damage response (G).

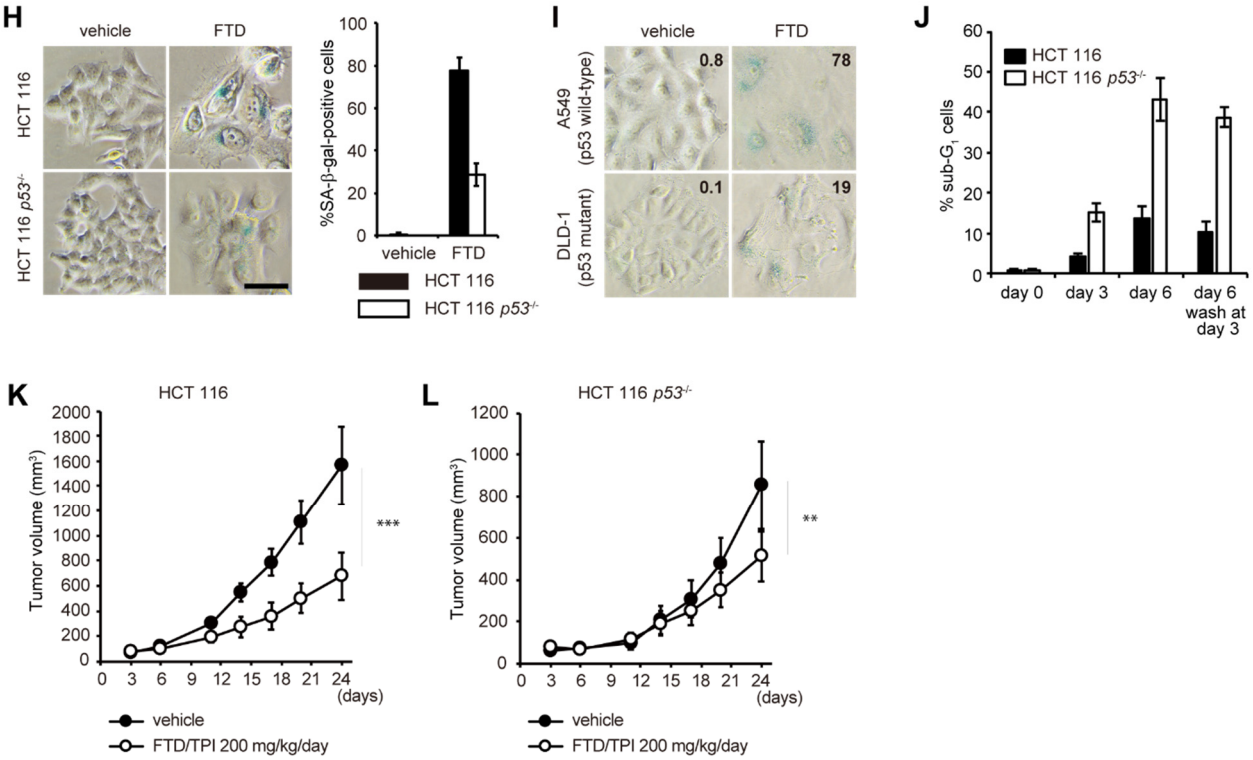

Figure 2-5: Outcomes of Cells Cultured in the Presence of FTD. (Continued)

(H) SA-β-gal activity of HCT 116 and HCT 116 *p53*$^{-/-}$ cells on day 3; The black bar represents 50 µm. The graph shows the percentage of SA-β-gal–positive cells. Error bars represent the SD of three independent experiments. (I) SA-β-gal activity of A549 and DLD-1 cells cultured in the presence of the IC_{50} concentration of FTD. (J) Sub-G_1 population. HCT 116 and HCT 116 *p53*$^{-/-}$ cells were cultured in the presence of 3 µmol/L FTD and harvested on the indicated days. Ethanol-fixed samples were stained with propidium iodide and the percentage of sub-G_1 cells was measured. Error bars, the SD of three independent experiments. (K, L) Growth curve of HCT 116 (K) and HCT 116 *p53*$^{-/-}$ (L) xenografts. Error bars represent the SD of 6 individual mice. Statistical analysis was done at day 24. Unpaired *t* test. (**, $P < 0.01$; ***, $P < 0.001$).

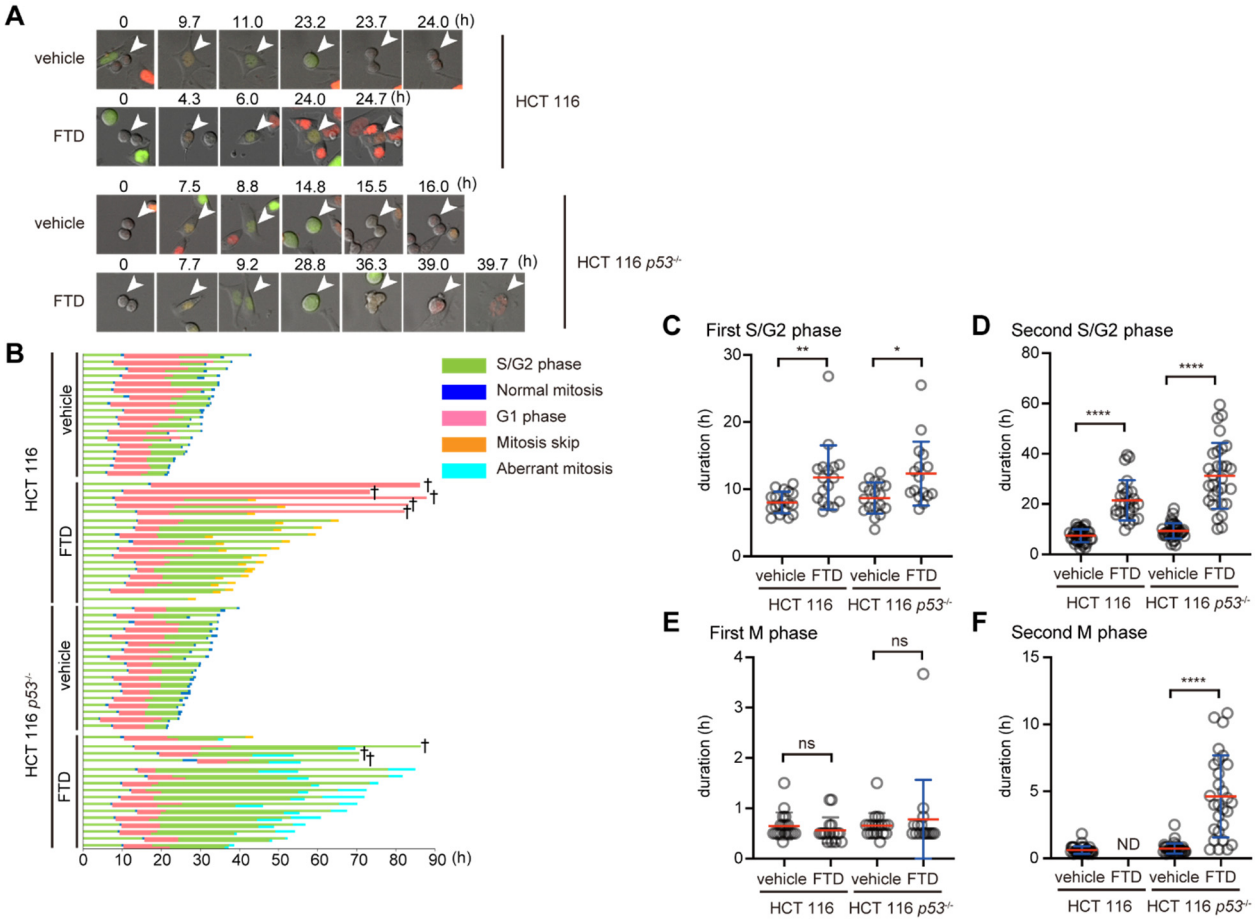

Figure 2-6: Single-cell Live Imaging of Fucci Cells in Response to FTD.

(A) Representative images of HCT 116-Fucci and HCT 116 *p53*$^{-/-}$-Fucci cells, which were cultured in the presence or absence of 3 μmol/L FTD. Arrowheads indicate identical cells at each time point. (B) Cell-cycle phase and duration in HCT 116-Fucci and HCT 116 *p53*$^{-/-}$-Fucci cells, which were cultured in the presence or absence of 3 μmol/L FTD. Each bar represents one cell that was in G_1 phase (red color) at the start point. †, analysis terminated. Scattered plots of duration of the first (C) and the second S-G_2 phase (D), and the first (E) and the second M phase (F). Red lines and blue whiskers denote means and SD, respectively. Mann–Whitney *U* test. (*, $P < 0.05$; **, $P < 0.01$; ****, $P < 0.0001$; ns, not significant; ND, not detected).

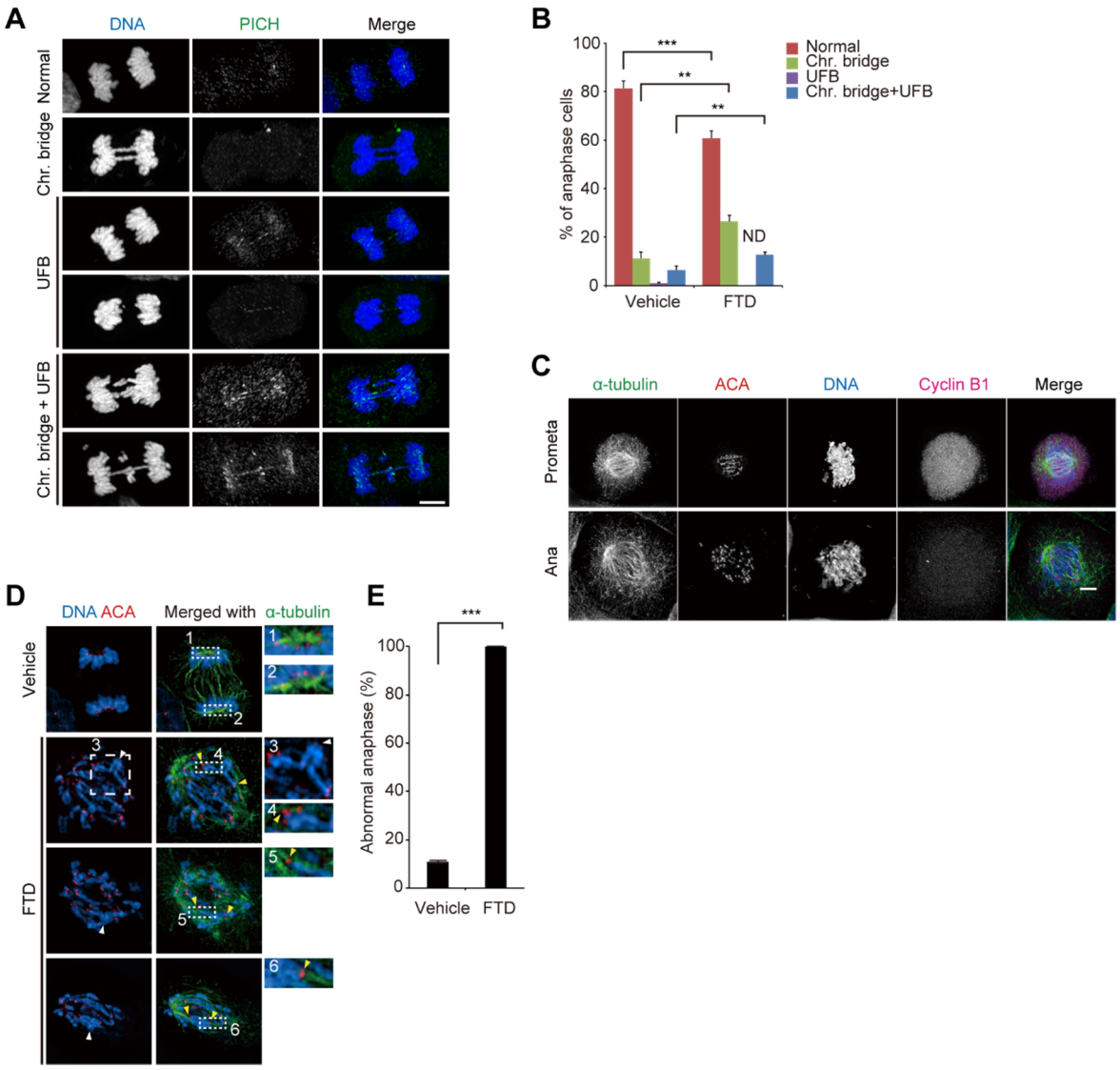

Figure 2-7: Aberrant Chromosomal Structures of HCT 116 *p53*$^{-/-}$ Cells in Response to FTD.

(A) Representative immunofluorescence images of anaphase HCT 116 *p53*$^{-/-}$ cells, which were either untreated (Normal, and UFB) or cultured in the presence of 3 μmol/L FTD and 9 μmol/L RO-3306 for 16 hours and released into fresh media for 50 minutes (Chr. Bridge, and Chr. Bridge + UFB). (B) Quantitative data of A. Error bars represent SD of three independent experiments. Unpaired *t* test. (**, $P < 0.01$; ***, $P < 0.001$). (C) Fluorescence immunostaining of α-tubulin, centromere (ACA), cyclin B1, and DNA in proliferating HCT 116 cells at prometaphase (Prometa) and anaphase (Ana). (D) Representative super-resolution immunofluorescence images of anaphase HCT 116 *p53*$^{-/-}$ cells, which were cultured in the presence of 3 μmol/L FTD for 60 hours. The centromeres (ACA) captured by spindles are indicated by yellow arrowheads. Sister chromatid pairs with entangled chromosome arms are indicated by white arrowheads. Enlarged images of rectangles with dashed lines are shown in the inlets. (E) Quantitative data of abnormal anaphase. Error bars, SD of three independent experiments. Unpaired *t* test. (***, $P < 0.001$).

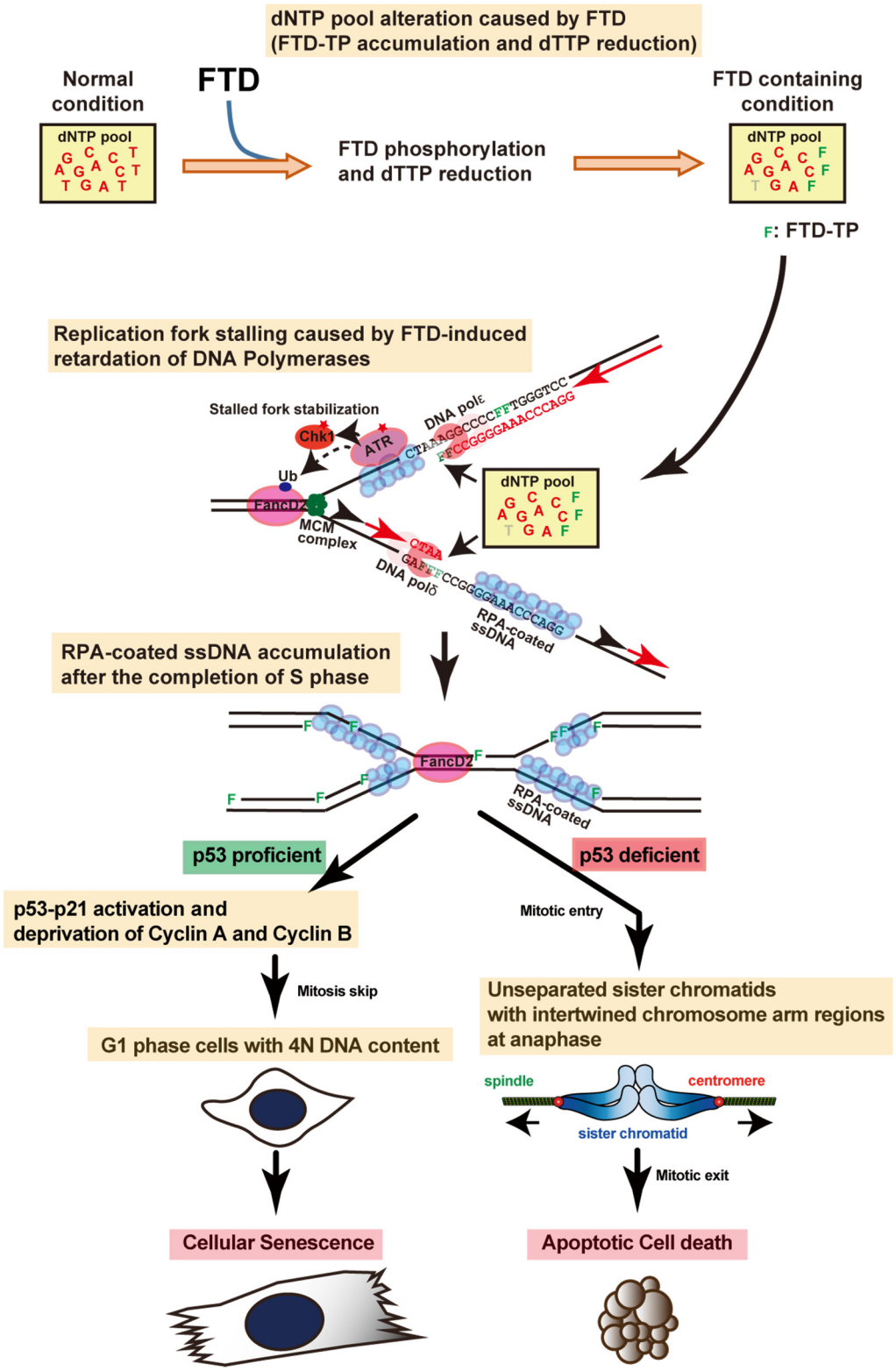

Figure 2-8: Schematic Model of the Effect of FTD and Cell Fate Decision in Tumor Cells.

See text for details.

General Discussion

In this study, I analyzed the molecular determinant of cell fate induced by an antimetabolite, FTD. First, to verify the importance of TK1 for cytotoxicity of FTD, I established *TK1*-specific-deficient and TK1-expression-inducible human cancer cell lines and illustrated that TK1 was an indispensable molecule for FTD to exert antitumor effect. In clinical situations, TK1 is assumed as a prognostic factor, because high *TK1* expression is related to poor prognosis in various cancers [27-31]. FTD/TPI treatment was indicated to be highly effective against *TK1*-high-expressing tumor [32, 33]. These data support the clinical findings. Second, FTD was incorporated into DNA by DNA polymerase, but the efficiency was lower than that for thymidine, the original substrate, thus FTD generated continuous DRS. Moreover, FTD caused DRS when it served as a template for DNA replication. Thus, FTD induced DRS sustainably. Finally, the DRS caused two different phenotypes according to the cellular p53 status. In the event that p53 was wild-type, cellular senescence was induced; alternatively, if p53 was deficient, cells apoptosed following mitotic catastrophe. In summary, FTD is phosphorylated at cytosol by TK1 and reduces dTTP after uptake into the cells. The phosphorylated FTD (FTD-TP) induces DRS after incorporation into DNA by DNA polymerases. The DRS induces cellular senescence in p53 proficient cells via p53-p21 activation, and apoptosis in p53 deficient cells.

Some antimetabolites such as gemcitabine or cytarabine are also incorporated into DNA by DNA polymerase; however, these drugs halted subsequent DNA elongation from the incorporated aberrant nucleotide [4, 5], resulting in cell cycle arrest in S phase [72]. As was just described, FTD has been suggested to have a structure similar to that of other antimetabolites but has a completely different effect. I established and analyzed p53-KO cell line; however, various mutations of p53 are gain-of-function type, and therefore, further investigation is required. Moreover, while FTD exerted equivalent antitumor effect on nude mice bearing subcutaneous HCT 116 or HCT 116 *p53*$^{-/-}$ xenografts, the cellular phenotypes induced by FTD *in vivo* remain unclear. Since cancer cells are in a completely different environment *in vivo* than *in vitro*, detailed analyses of *in vivo* xenografts are essential. UFBs, one of the inseparable structures of sister chromatids, were observed in HCT 116 *p53*$^{-/-}$ cells treated with FTD.

UFB is rarely observed in normal cells and are currently being studied extensively. CFS, a certain region of genome, is hard to replicate, and cell cycle was not arrested even if CFS was

not completely replicated. Normally, sister chromatids segregate into two poles at M phase. In contrast, if DNA replication had not been completed, sister chromatids would be tied up by the UR-DNA, and the UR-DNA observed by immunofluorescence is called UFB. FTD was incorporated opposite adenine, and adenine- and thymidine-rich regions are considered CSFs [73-78], therefore, FTD seems to make CFS more unstable. Because FTD increased UFB, FTD was indicated as a tool to understand the cellular response against CFS or UFB.

TK1 expression level is higher in cancer cells than normal cells; simultaneously, p53 is mutated in many types of cancer and the mutation is related to drug resistance. These results indicate that FTD/TPI is efficient to broad range of cancer.

DNA replication and DNA repair have been analyzed for a long time. In addition, antimetabolites have been used to treat different tumors clinically for decades. However, these are not completely elucidated. In this research, I focused on the differences in cellular response against FTD of p53-proficient cells and p53-null cells. More comprehensive mechanism of cellular response to various types of DRS can be unveiled by conducting phenotypic analyses of the cells expressing p53 gain-of-function mutants against FTD and other antimetabolites such as gemcitabine or cytarabine. I found out that FTD induces apoptosis in p53-deficient cell lines. It is known that there are various mutant p53 genes which affect on the activity of p53 protein. Although FTD sensitivity of p53-mutant cells have not been analyzed yet, it is assumed that some of the mutated cells are also sensitive to FTD and FTD induces apoptosis in them, too. Since many of p53-mutant cells are resistant to many of anti-cancer drugs, the apoptosis-induction potency in p53-mutantcells might be an advantage of FTD to other drugs.

Furthermore, by analyzing the anti-tumor effect and the phenotype induced by FTD on in vivo models that retain the heterogeneous microenvironment, such as patient derived xenograft or carcinogenesis animal model, the clinical effect of FTD can be predicted more accurately. Overall, this study provides valuable insight for all of these applied studies.

Acknowledgements

I am deeply grateful to Professor Hidekazu Kuwayama at the University of Tsukuba for his peer-review and invaluable advice.

I express my deepest appreciation to Dr. Yoshihiko Maehara for providing me the opportunity to carry out this study. I also express immense gratitude to Dr. Hiroyuki Kitao and Dr. Makoto Iimori for supervising my work and their valuable suggestions, contributions, and support.

I acknowledge Dr. Ryo Fujisawa, Dr. Tomomi Morikawa-Ichinose, Dr. Shinichiro Niimi, Dr. Takeshi Wakasa, Mr. Hiroshi Tsukihara, Dr. Hiroshi Saeki, Dr. Eiji Oki, Dr. Daisuke Miura, and Dr. Toshiki Tsurimoto for their helpful discussions and support throughout the study.

I deeply thank Ms. Masako Kosugi, Tomomi Takada, Naoko Katakura, and Atsuko Yamaguchi for their expert technical assistance.

I am greatly indebted to all the people who made this thesis possible. I am also grateful to the supervisors and colleagues at Taiho Pharmaceutical Co., Ltd. for their understanding and support during my doctoral program.

Finally, I would like to appreciate my family for their constant support of me and my work at the University of Tsukuba.

References

1. Johmura, Y., et al., *Necessary and sufficient role for a mitosis skip in senescence induction.* Mol Cell, 2014. **55**(1): p. 73-84.
2. Alvarado-Ortiz, E., et al., *Mutant p53 Gain-of-Function: Role in Cancer Development, Progression, and Therapeutic Approaches.* Front Cell Dev Biol, 2020. **8**: p. 607670.
3. Kitao, H., et al., *DNA replication stress and cancer chemotherapy.* Cancer Sci, 2018. **109**(2): p. 264-271.
4. Huang, P., et al., *Action of 2',2'-difluorodeoxycytidine on DNA synthesis.* Cancer Res, 1991. **51**(22): p. 6110-7.
5. Kukhanova, M., et al., *L- and D-enantiomers of 2',3'-dideoxycytidine 5'-triphosphate analogs as substrates for human DNA polymerases. Implications for the mechanism of toxicity.* J Biol Chem, 1995. **270**(39): p. 23055-9.
6. Chen, Y.W., et al., *A novel role of DNA polymerase eta in modulating cellular sensitivity to chemotherapeutic agents.* Mol Cancer Res, 2006. **4**(4): p. 257-65.
7. Mayer, R.J., et al., *Randomized trial of TAS-102 for refractory metastatic colorectal cancer.* N Engl J Med, 2015. **372**(20): p. 1909-19.
8. Shitara, K., et al., *Trifluridine/tipiracil versus placebo in patients with heavily pretreated metastatic gastric cancer (TAGS): a randomised, double-blind, placebo-controlled, phase 3 trial.* Lancet Oncol, 2018. **19**(11): p. 1437-1448.
9. Emura, T., et al., *An optimal dosing schedule for a novel combination antimetabolite, TAS-102, based on its intracellular metabolism and its incorporation into DNA.* Int J Mol Med, 2004. **13**(2): p. 249-55.
10. Tanaka, N., et al., *Repeated oral dosing of TAS-102 confers high trifluridine incorporation into DNA and sustained antitumor activity in mouse models.* Oncol Rep, 2014. **32**(6): p. 2319-26.
11. Sakamoto, K., et al., *Crucial roles of thymidine kinase 1 and deoxyUTPase in incorporating the antineoplastic nucleosides trifluridine and 2'-deoxy-5-fluorouridine into DNA.* Int J Oncol, 2015. **46**(6): p. 2327-34.
12. Matsuoka, K., et al., *Trifluridine Induces p53-Dependent Sustained G2 Phase Arrest with Its Massive Misincorporation into DNA and Few DNA Strand Breaks.* Mol Cancer Ther, 2015. **14**(4): p. 1004-13.
13. Lin, P.F., S.Y. Zhao, and F.H. Ruddle, *Genomic cloning and preliminary characterization of the human thymidine kinase gene.* Proc Natl Acad Sci U S A, 1983. **80**(21): p. 6528-32.
14. Eriksson, S., et al., *Comparison of the substrate specificities of human thymidine kinase 1 and 2 and deoxycytidine kinase toward antiviral and cytostatic nucleoside analogs.* Biochem Biophys Res Commun, 1991. **176**(2): p. 586-92.
15. Johansson, N.G. and S. Eriksson, *Structure-activity relationships for phosphorylation of nucleoside analogs to monophosphates by nucleoside kinases.* Acta Biochim Pol, 1996. **43**(1): p. 143-60.
16. Murakami, Y., et al., *Different mechanisms of acquired resistance to fluorinated pyrimidines in human colorectal cancer cells.* Int J Oncol, 2000. **17**(2): p. 277-83.
17. Temmink, O.H., et al., *Intracellular thymidylate synthase inhibition by trifluorothymidine in FM3A cells.* Nucleosides Nucleotides Nucleic Acids, 2004. **23**(8-9): p. 1491-4.

18. Naito, Y., et al., *CRISPRdirect: software for designing CRISPR/Cas guide RNA with reduced off-target sites.* Bioinformatics, 2015. **31**(7): p. 1120-3.
19. Cong, L., et al., *Multiplex genome engineering using CRISPR/Cas systems.* Science, 2013. **339**(6121): p. 819-23.
20. Edahiro, K., et al., *Thymidine Kinase 1 Loss Confers Trifluridine Resistance without Affecting 5-Fluorouracil Metabolism and Cytotoxicity.* Mol Cancer Res, 2018. **16**(10): p. 1483-1490.
21. Dobrovolsky, V.N., et al., *Mice deficient for cytosolic thymidine kinase gene develop fatal kidney disease.* Mol Genet Metab, 2003. **78**(1): p. 1-10.
22. Dobrovolsky, V.N., et al., *Effect of arylformamidase (kynurenine formamidase) gene inactivation in mice on enzymatic activity, kynurenine pathway metabolites and phenotype.* Biochim Biophys Acta, 2005. **1724**(1-2): p. 163-72.
23. Kitao, H., et al., *The antibodies against 5-bromo-2'-deoxyuridine specifically recognize trifluridine incorporated into DNA.* Sci Rep, 2016. **6**: p. 25286.
24. Takahashi, K., et al., *Contribution of equilibrative nucleoside transporter(s) to intestinal basolateral and apical transports of anticancer trifluridine.* Biopharm Drug Dispos, 2018. **39**(1): p. 38-46.
25. Takahashi, K., et al., *Involvement of Concentrative Nucleoside Transporter 1 in Intestinal Absorption of Trifluridine Using Human Small Intestinal Epithelial Cells.* J Pharm Sci, 2015. **104**(9): p. 3146-53.
26. Gordon, H.L., et al., *Comparative study of the thymidine kinase and thymidylate kinase activities and of the feedbach inhibition of thymidine kinase in normal and neoplastic human tissue.* Cancer Res, 1968. **28**(10): p. 2068-77.
27. He, Q., et al., *Thymidine kinase 1 in serum predicts increased risk of distant or loco-regional recurrence following surgery in patients with early breast cancer.* Anticancer Res, 2006. **26**(6C): p. 4753-9.
28. Kolberg, M., et al., *Protein expression of BIRC5, TK1, and TOP2A in malignant peripheral nerve sheath tumours--A prognostic test after surgical resection.* Mol Oncol, 2015. **9**(6): p. 1129-39.
29. Wang, J., et al., *Thymidine kinase 1 expression in ovarian serous adenocarcinoma is superior to Ki-67: A new prognostic biomarker.* Tumour Biol, 2017. **39**(6): p. 1010428317706479.
30. Xu, Y., et al., *Thymidine kinase 1 is a better prognostic marker than Ki-67 for pT1 adenocarcinoma of the lung.* Int J Clin Exp Med, 2014. **7**(8): p. 2120-8.
31. Xu, Y., et al., *High thymidine kinase 1 (TK1) expression is a predictor of poor survival in patients with pT1 of lung adenocarcinoma.* Tumour Biol, 2012. **33**(2): p. 475-83.
32. Yoshino, T., et al., *Effect of thymidine kinase 1 expression on prognosis and treatment outcomes in refractory metastatic colorectal cancer: Results from two randomized studies of TAS-102 versus a placebo.* Journal of Clinical Oncology, 2017. **35**: p. 1.
33. Yoshino, T., et al., *Relationship Between Thymidine Kinase 1 Expression and Trifluridine/Tipiracil Therapy in Refractory Metastatic Colorectal Cancer: A Pooled Analysis of 2 Randomized Clinical Trials.* Clin Colorectal Cancer, 2018. **17**(4): p. e719-e732.
34. Techer, H., et al., *The impact of replication stress on replication dynamics and DNA damage in vertebrate cells.* Nat Rev Genet, 2017. **18**(9): p. 535-550.

35. Halazonetis, T.D., V.G. Gorgoulis, and J. Bartek, *An oncogene-induced DNA damage model for cancer development.* Science, 2008. **319**(5868): p. 1352-5.
36. Dobbelstein, M. and C.S. Sorensen, *Exploiting replicative stress to treat cancer.* Nat Rev Drug Discov, 2015. **14**(6): p. 405-23.
37. Cimprich, K.A. and D. Cortez, *ATR: an essential regulator of genome integrity.* Nat Rev Mol Cell Biol, 2008. **9**(8): p. 616-27.
38. Ceccaldi, R., P. Sarangi, and A.D. D'Andrea, *The Fanconi anaemia pathway: new players and new functions.* Nat Rev Mol Cell Biol, 2016. **17**(6): p. 337-49.
39. Ishiai, M., et al., *FANCI phosphorylation functions as a molecular switch to turn on the Fanconi anemia pathway.* Nat Struct Mol Biol, 2008. **15**(11): p. 1138-46.
40. Andreassen, P.R., A.D. D'Andrea, and T. Taniguchi, *ATR couples FANCD2 monoubiquitination to the DNA-damage response.* Genes Dev, 2004. **18**(16): p. 1958-63.
41. Durkin, S.G. and T.W. Glover, *Chromosome fragile sites.* Annu Rev Genet, 2007. **41**: p. 169-92.
42. Chan, K.L., et al., *Replication stress induces sister-chromatid bridging at fragile site loci in mitosis.* Nat Cell Biol, 2009. **11**(6): p. 753-60.
43. Marusyk, A., et al., *p53 mediates senescence-like arrest induced by chronic replicational stress.* Mol Cell Biol, 2007. **27**(15): p. 5336-51.
44. Ewald, J.A., et al., *Therapy-induced senescence in cancer.* J Natl Cancer Inst, 2010. **102**(20): p. 1536-46.
45. Ewald, B., D. Sampath, and W. Plunkett, *Nucleoside analogs: molecular mechanisms signaling cell death.* Oncogene, 2008. **27**(50): p. 6522-37.
46. Bijnsdorp, I.V., et al., *Trifluorothymidine induces cell death independently of p53.* Nucleosides Nucleotides Nucleic Acids, 2008. **27**(6): p. 699-703.
47. Nieminuszczy, J., R.A. Schwab, and W. Niedzwiedz, *The DNA fibre technique - tracking helicases at work.* Methods, 2016. **108**: p. 92-8.
48. Murakami, T., et al., *Stable interaction between the human proliferating cell nuclear antigen loader complex Ctf18-replication factor C (RFC) and DNA polymerase {epsilon} is mediated by the cohesion-specific subunits, Ctf18, Dcc1, and Ctf8.* J Biol Chem, 2010. **285**(45): p. 34608-15.
49. Narita, T., et al., *Human replicative DNA polymerase delta can bypass T-T (6-4) ultraviolet photoproducts on template strands.* Genes Cells, 2010. **15**(12): p. 1228-39.
50. Shiomi, Y., et al., *A second proliferating cell nuclear antigen loader complex, Ctf18-replication factor C, stimulates DNA polymerase eta activity.* J Biol Chem, 2007. **282**(29): p. 20906-14.
51. Kiyonari, S., et al., *The 1,2-Diaminocyclohexane Carrier Ligand in Oxaliplatin Induces p53-Dependent Transcriptional Repression of Factors Involved in Thymidylate Biosynthesis.* Mol Cancer Ther, 2015. **14**(10): p. 2332-42.
52. Arakawa, H., D. Lodygin, and J.M. Buerstedde, *Mutant loxP vectors for selectable marker recycle and conditional knock-outs.* BMC Biotechnol, 2001. **1**: p. 7.
53. Iimori, M., et al., *Phosphorylation of EB2 by Aurora B and CDK1 ensures mitotic progression and genome stability.* Nat Commun, 2016. **7**: p. 11117.
54. Okamoto, Y., et al., *Replication stress induces accumulation of FANCD2 at central region of large fragile genes.* Nucleic Acids Res, 2018. **46**(6): p. 2932-2944.
55. Krenning, L., et al., *Transient activation of p53 in G2 phase is sufficient to induce senescence.* Mol Cell, 2014. **55**(1): p. 59-72.

56. Ercilla, A., et al., *Physiological Tolerance to ssDNA Enables Strand Uncoupling during DNA Replication.* Cell Rep, 2020. **30**(7): p. 2416-2429 e7.
57. Lossaint, G., et al., *FANCD2 binds MCM proteins and controls replisome function upon activation of s phase checkpoint signaling.* Mol Cell, 2013. **51**(5): p. 678-90.
58. Sakaue-Sawano, A., et al., *Visualizing spatiotemporal dynamics of multicellular cell-cycle progression.* Cell, 2008. **132**(3): p. 487-98.
59. Vassilev, L.T., et al., *Selective small-molecule inhibitor reveals critical mitotic functions of human CDK1.* Proc Natl Acad Sci U S A, 2006. **103**(28): p. 10660-5.
60. Temmink, O.H., et al., *Therapeutic potential of the dual-targeted TAS-102 formulation in the treatment of gastrointestinal malignancies.* Cancer Sci, 2007. **98**(6): p. 779-89.
61. Kroep, J.R., et al., *Sequence dependent effect of paclitaxel on gemcitabine metabolism in relation to cell cycle and cytotoxicity in non-small-cell lung cancer cell lines.* Br J Cancer, 2000. **83**(8): p. 1069-76.
62. Debatisse, M., et al., *Common fragile sites: mechanisms of instability revisited.* Trends Genet, 2012. **28**(1): p. 22-32.
63. Tubbs, A., et al., *Dual Roles of Poly(dA:dT) Tracts in Replication Initiation and Fork Collapse.* Cell, 2018. **174**(5): p. 1127-1142 e19.
64. Toledo, L.I., et al., *ATR prohibits replication catastrophe by preventing global exhaustion of RPA.* Cell, 2013. **155**(5): p. 1088-103.
65. Tsuda, M., et al., *The dominant role of proofreading exonuclease activity of replicative polymerase epsilon in cellular tolerance to cytarabine (Ara-C).* Oncotarget, 2017. **8**(20): p. 33457-33474.
66. Feng, L., et al., *Role of p53 in cellular response to anticancer nucleoside analog-induced DNA damage.* Int J Mol Med, 2000. **5**(6): p. 597-604.
67. Jackson, J.G., et al., *p53-mediated senescence impairs the apoptotic response to chemotherapy and clinical outcome in breast cancer.* Cancer Cell, 2012. **21**(6): p. 793-806.
68. Milanovic, M., et al., *Senescence-associated reprogramming promotes cancer stemness.* Nature, 2018. **553**(7686): p. 96-100.
69. Matsuoka, K., et al., *Trifluridine/tipiracil overcomes the resistance of human gastric 5-fluorouracil-refractory cells with high thymidylate synthase expression.* Oncotarget, 2018. **9**(17): p. 13438-13450.
70. Temmink, O.H., et al., *Trifluorothymidine resistance is associated with decreased thymidine kinase and equilibrative nucleoside transporter expression or increased secretory phospholipase A2.* Mol Cancer Ther, 2010. **9**(4): p. 1047-57.
71. Sabapathy, K. and D.P. Lane, *Therapeutic targeting of p53: all mutants are equal, but some mutants are more equal than others.* Nat Rev Clin Oncol, 2018. **15**(1): p. 13-30.
72. Auer, H., et al., *Characterisation of genotoxic properties of 2',2'-difluorodeoxycytidine.* Mutat Res, 1997. **393**(1-2): p. 165-73.
73. Zhang, H. and C.H. Freudenreich, *An AT-rich sequence in human common fragile site FRA16D causes fork stalling and chromosome breakage in S. cerevisiae.* Mol Cell, 2007. **27**(3): p. 367-79.
74. Kaushal, S. and C.H. Freudenreich, *The role of fork stalling and DNA structures in causing chromosome fragility.* Genes Chromosomes Cancer, 2019. **58**(5): p. 270-283.

75. Kaushal, S., et al., *Sequence and Nuclease Requirements for Breakage and Healing of a Structure-Forming (AT)n Sequence within Fragile Site FRA16D.* Cell Rep, 2019. **27**(4): p. 1151-1164 e5.
76. Irony-Tur Sinai, M., et al., *AT-dinucleotide rich sequences drive fragile site formation.* Nucleic Acids Res, 2019. **47**(18): p. 9685-9695.
77. Walsh, E., et al., *Mechanism of replicative DNA polymerase delta pausing and a potential role for DNA polymerase kappa in common fragile site replication.* J Mol Biol, 2013. **425**(2): p. 232-43.
78. Li, S. and X. Wu, *Common fragile sites: protection and repair.* Cell Biosci, 2020. **10**: p. 29.